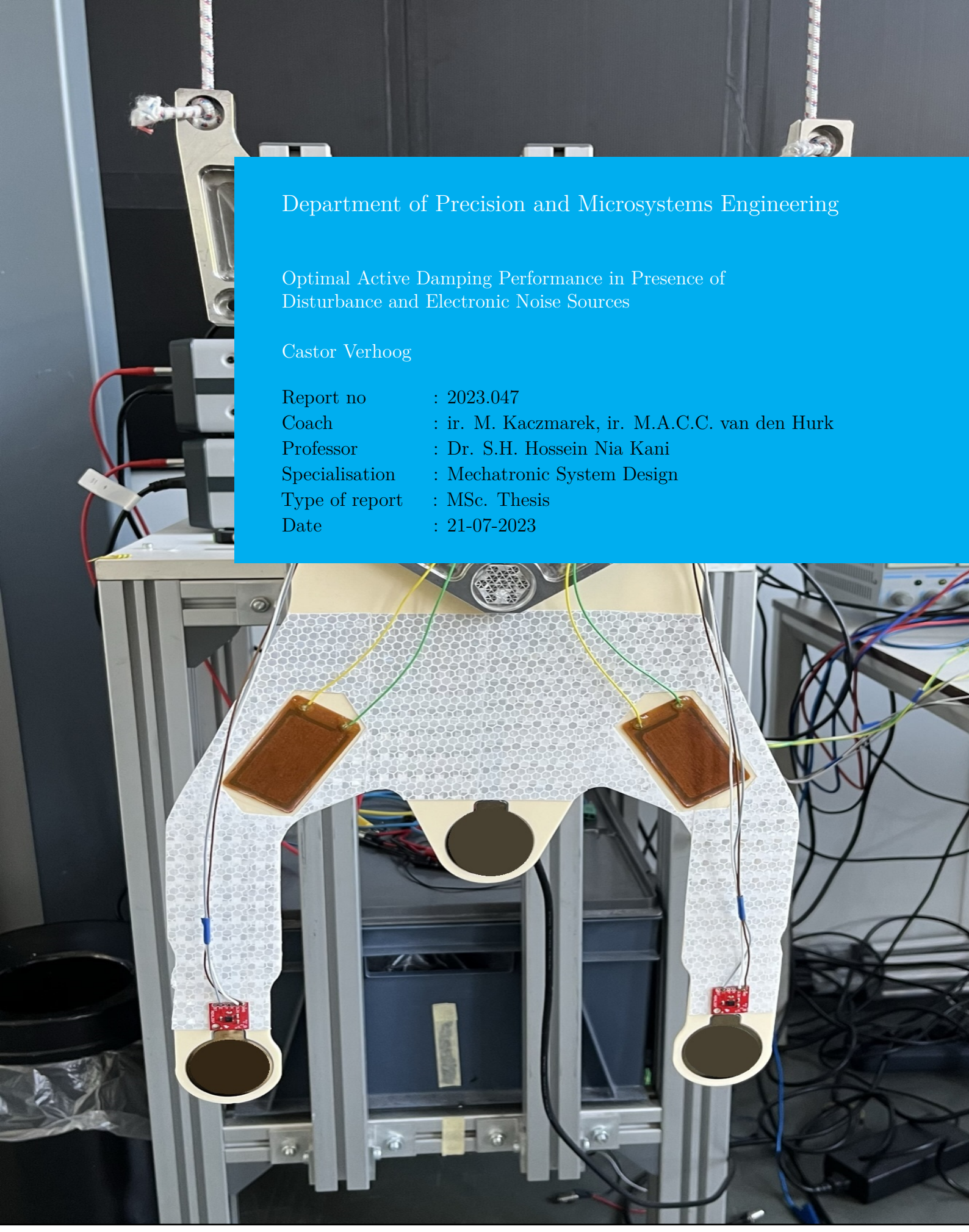

Department of Precision and Microsystems Engineering

Optimal Active Damping Performance in Presence of Disturbance and Electronic Noise Sources

Castor Verhoog

Report no	: 2023.047
Coach	: ir. M. Kaczmarek, ir. M.A.C.C. van den Hurk
Professor	: Dr. S.H. Hossein Nia Kani
Specialisation	: Mechatronic System Design
Type of report	: MSc. Thesis
Date	: 21-07-2023

TU Delft Delft University of Technology

Challenge the future

MSc. Thesis

Optimal Active Damping Performance in Presence of Disturbance and Electronic Noise Sources

by

Castor Verhoog

Student number:	4676491	
Project duration:	October 10, 2022 – July 21, 2023	
Supervisors:	dr. S.H. Hossein Nia Kani	TU Delft
	ir. M.B. Kaczmarek,	TU Delft
	ir. M.A.C.C. van den Hurk	VDL ETG B.V.

An electronic version of this thesis is available at `http://repository.tudelft.nl/`.

TU Delft

Preface

Before you lies the MSc. Thesis I have worked on for the past year. The thesis contains the research of a Active Vibration Control setup and the practical issues that such a system encounters. I have written this thesis for the Master High-Tech Engineering at the Delft University of Technology.

I take great pride in what I have achieved this year. Not only in the results, but also in what I have learnt about a subject that truly interests me. As the start of my career stands before me, I am glad that I have been busy during my student time in Delft with finding what I love to do. Just as this thesis concludes my time as a student in Delft, it starts my path of learning more and more about the subject of mechatronics during my career.

I wish the reader much joy in learning about the journey I have had in the past year.

Castor Verhoog
Delft, July 2023

Summary

Vibration attenuation in lightly damped blade-like systems such as cantilevers or end-effectors of robot manipulators can be dampened using Active Vibration Control (AVC). Piezoelectric patches in a collocated setup measure and control the bending modes of such a cantilever system using Positive Position Feedback (PPF). Tuning methods for PPF are based on optimisations for maximum disturbance rejection and disregard the presence of electronic noise. However, because electronic noise is amplified by controllers with high gains, it can become a significant error source in the system. In this paper, the effect of noise amplification is investigated for blade-like AVC systems. It is shown that there is a trade-off in the total dynamic error between vibration attenuation and noise amplification. An optimisation of this trade-off is proposed, which is performed on an industrial example of a blade-like system and validated experimentally. The optimisation shows clear improvement over traditional tuning methods that disregard the presence and effect of noise.

Contents

Nomenclature

Abbreviations

Abbreviation	Definition
AVC	Active Vibration Control
CPS	Cumulative Power Spectrum
DEB	Dynamic Error Budgeting
DVF	Direct Velocity Feedback
FRF	Frequency Response Function
HAC	High Authority Control
IRC	Integral Resonant Control
LAC	Low Authority Control
NDF	Negative Derivative Feedback
NPF	Negative Positional Feedback
PPF	Positive Positional Feedback
PSD	Power Spectral Density
SA	Sensor-Actuator

1

Introduction

Silicon chip manufacturers are experiencing an ever-growing demand for smaller and faster chips, forming the basis of Internet of Things and Artificial Intelligence. As the demand for more and faster chips grows, the machines that make these chips must grow in speed and precision.

As the highly dynamic precision systems which make up the semiconductor industry become quicker and more precise, problems with unwanted vibrations arise. Vibrations that previously were negligible now have to be accounted for by isolating or suppressing them. The field of vibration suppression has grown a lot in the past decades, and examples of vibration suppression are common in the semiconductor industry. While passive damping methods such as Tuned Mass Damping or Constrained Layer Damping are still widely used, *Active Vibration Control (AVC)* is used where better performance, adaptability or easier implementation is required [1].

AVC has been applied in structures at least since the introduction of direct velocity feedback control [2] in large space structures. Since then, the field has been extensively covered in papers and books [3, 4]. Most papers introduce some kind of performance increase, focused on increasing disturbance rejection. Positive position feedback introduced performance increases for any kind of collocated system, as it prevents spill-over problems due to amplification of high-frequency dynamics. [4, 5] showed how the distance between the pole and transmission zero in collocated systems links to maximum reachable damping for SISO and MIMO systems. Following this principe, adding a feed-through term increases this distance and thus increases damping performance [6].

Although improvements on AVC have been about increasing the disturbance rejection as much as possible, in practice, an AVC system encounters practical issues that can limit the maximum performance. The most common practical issue is electronic noise generated by the electronics responsible for the measurements and control of the system. High controller gains can consequently amplify electronic noise and create an error greater than the original disturbance, depending on the noise/disturbance ratio. Although it is a common issue, few literature exists about the issue of noise amplification in an AVC blade-like system.

Noise amplification can be considered by using *Dynamic Error Budgeting (DEB)* to balance different disturbance and noise sources. DEB considers the total dynamic error that propagates through the system from these disturbances and this dynamic error is then minimised. This is often performed in Vibration Isolation systems [7, 8].

In this thesis, the effect of noise on an AVC system is analysed by applying DEB. It is shown that traditional tuning methods can amplify the electronic noise to create an error greater than the original disturbance. The trade-off between the disturbance and noise is analysed to propose an optimal solution, which is validated in an experimental setup. In the following section, the problem that forms the motivation of the project is explained.

1.1. Problem Definition

ASML N.V. provides the world with high through-put lithography machines that make the semiconductor industry possible. These room-sized machines create the raw silicon chips found in every device. In addition to high-speed lithography, the machine handles silicon wafers with great precision and speed. VDL ETG B.V. designs and manufactures the wafer handling system part of the machine.

The wafer handling system is designed to move silicon wafers from an atmospheric environment to the vacuum environment of the lithography machine through an airlock, called the vacuum vessel. One system moves the wafers from the atmospheric pick-up spot to the vacuum vessel and a second system moves them from the vacuum vessel into the machine. Inside the vacuum vessel is a wafer prealigner, which aligns the wafer to a known position. A robot manipulator then docks with the prealigner, picks up the wafer, and moves the wafer onto the wafer stage. The robot manipulator end-effector is shown in Figure 1.1. The end-effector is a thin ceramic plate, which is a stiff, lightly damped structure.

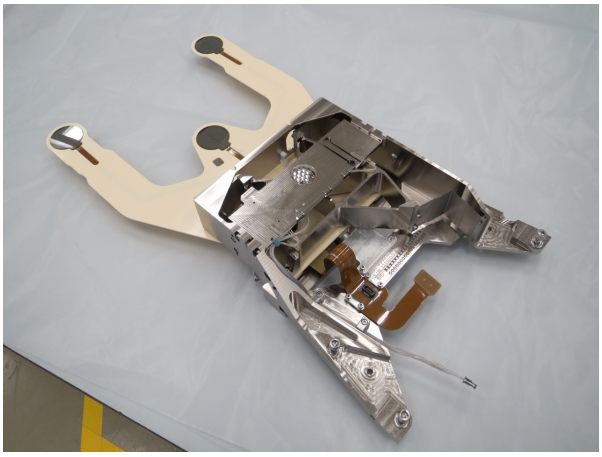

Figure 1.1: The robot manipulator's end-effector, which picks up the silicon wafers from the pre-aligner inside the vacuum vessel/airlock.

With docking between the robot manipulator and pre-aligner, the docking impact induces vibrations in the lightly-damped end-effector. While the end-effector is moving due to these vibrations, the wafer can not be picked up as there is a risk of the wafer shifting and reduced pick-up accuracy. Because of this, the machine has to either wait for vibrations to settle before the wafer can be picked up or decrease its movement speed entirely to decrease the docking impact. This waiting time limits the total throughput of the machine. Increasing end-effector damping would reduce the settling time and thus increase the machine's throughput.

1.2. Previous work and initial problem investigation

This thesis continues the work of M. El Ajjaj [9] from September 2021 to July 2022. The use of AVC was investigated and compared to the use of passive or semi-passive methods such as constrained layer damping, tuned mass damper, or piezoelectric shunting. The thesis of M. El Ajjaj finished with a proof of concept in which Positive Positional Feedback (PPF) was used as controller and a maximum modal damping of the largest mode of 3.3% was reached, as seen in Figure 1.2. Higher gains resulted in an unstable system. This instability could not be explained as its open-loop steady-state gain did not increase above 1, which is defined as the PPF stability condition [4]. The first step in solving the case study was explaining the instability of the system for PPF gains greater than 0.5. To do this, the system dynamics must be thoroughly identified.

In order to describe the system's dynamics, an extensive system identification was performed. The system is a Multi-Input Multi-Output (MIMO) system, with 3 inputs: the ground vibration source and 2x piezoelectric actuators, and 4 outputs: 2x piezoelectric sensors and 2x tip displacements. With 3 inputs and 4 outputs, the system can be described with 12 bode plots. Using a combination of a Polytec Scanning Doppler Vibrometer PSV-400 and a TI Delfino Launchpad F2837XD, these bode plots were

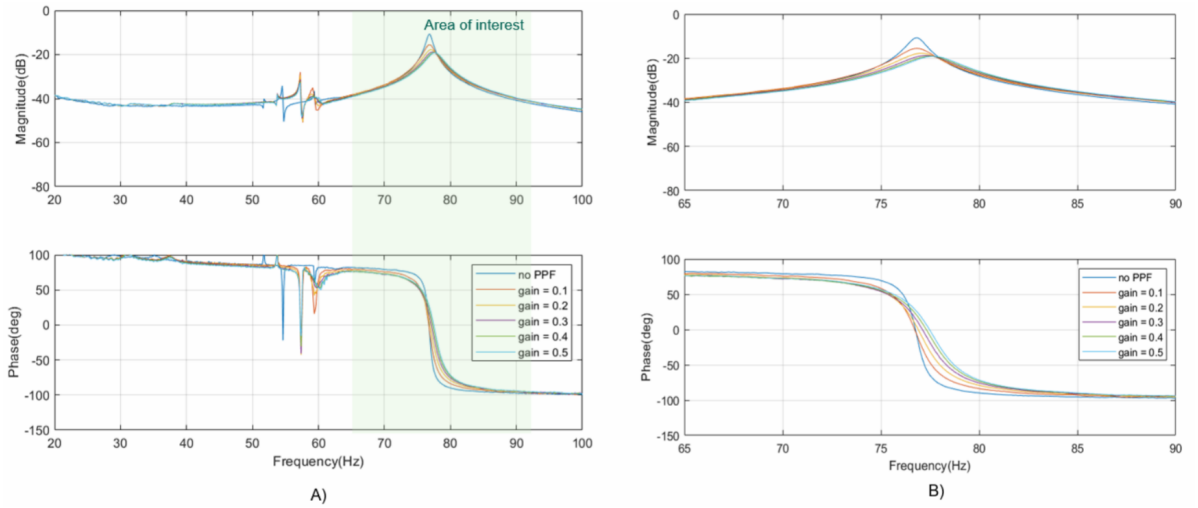

Figure 1.2: Result from [9] showing ~3.3% damping performance

generated. Investigating the bode plots of the collocated transfer functions between the piezoelectric actuator and the sensor patches, the problem is quickly observed. The collocated bode plots show an absolute steady-state gain of 2. This means that the open-loop transfer with a PPF controller of 0.5 already reaches a steady-state gain of 1. This means that increasing the PPF gain further will destabilise the system, as observed by M. El Ajjaj in her thesis. Thus, as the instability is explained, the next step is to investigate how to increase the performance of the total system.

In the literature study (Appendix A.5), different methods for increasing active damping performance were researched. Also, more importantly, it was investigated how the performance should be defined for an AVC system. The results of this literature forms the basis for the damping method used in the rest of the thesis. This includes the use of Dynamic Error Budgeting [7, 8] and the use of feed-through control to optimise active damping performance for a blade-like MIMO system [6].

1.3. Research Questions and Thesis Outline

In the thesis, the following research questions will be answered:

- How is performance defined in an Active Vibration Controlled system for a lightly damped, blade-like structure?
- What is an effective controller designed for optimising the performance of an Active Vibration Controlled system for a lightly damped, blade-like structure?

The following chapter will be the paper that resulted from the work done in this thesis. This paper was written according to the standards for the IEEE Transactions on Industrial Electronics journal. The paper includes the results and the main academic contribution. After the paper, the research questions of the thesis will be answered and the results are discussed in the Conclusion & Discussion chapter. In the Appendices, all the details about the final experimental setup can be read, as well as the literature study.

Optimal Active Damping Performance in Presence of Disturbance and Electronic Noise Sources

Department of Precision and Microsystems Engineering, Delft University of Technology

Vibration attenuation in lightly damped blade-like systems such as cantilevers or end-effectors of robot manipulators can be dampened using Active Vibration Control (AVC). Piezoelectric patches in a collocated setup measure and control the bending modes of such a cantilever system using Positive Position Feedback (PPF). Tuning methods for PPF are based on optimisations for maximum disturbance rejection and disregard the presence of electronic noise. However, because electronic noise is amplified by controllers with high gains, it can become a significant error source in the system. In this paper, the effect of noise amplification is investigated for blade-like AVC systems. It is shown that there is a trade-off in the total dynamic error between vibration attenuation and noise amplification. An optimisation of this trade-off is proposed, which is performed on an industrial example of a blade-like system and validated experimentally. The optimisation shows clear improvement over traditional tuning methods that disregard the presence and effect of noise.

I. Introduction

VIBRATIONS in mechanical systems can be caused by a variety of factors, including external disturbances, unbalanced forces, or electronic noise. The design of a system can create inherent dynamics that attenuate these vibrations. High-speed, high-precision motion systems are often designed to be stiff and lightweight, resulting in minimal modal damping. Excessively attenuated vibrations caused by insufficient damping can lead to problems, including mechanical malfunctions or, at best, a decrease in performance. Passive methods such as constrained layer damping or tuned mass damping can enhance modal damping, but *Active Vibration Control (AVC)* provides superior performance in a relatively smaller design volume [1].

In applications where AVC is implemented in thin, blade-like systems such as cantilevers, the bending harmonics tend to amplify ground disturbances at the tip. To mitigate this issue, piezoelectric patches are employed in an AVC system. A collocated configuration is used to achieve a transfer function with interlacing poles and zeros, keeping the phase between 0° and 180°. This is an important fundamental characteristic because it is possible to find a controller with guaranteed stability irrespective of changes in mass and stiffness distribution of the system[2]. *Positive Position Feedback (PPF)* is commonly employed in collocated blade-like systems, as it provides a high-frequency roll-off that minimises the risk of destabilising the system due to high-frequency dynamics.

PPF tuning methods consist of different control optimisation techniques such as H_2 or H_∞ optimisations, often performed assuming SISO mass-spring damping systems [3]. An important distinction between blade-like systems and SISO mass-spring damper AVC systems is that in blade-like systems, the controller *indirectly* dampens the performance function, where the performance function is defined by the transfer function from the ground disturbance to the displacement at the tip. PPF tuning methods are optimised for simplified single-mode systems, such as [4]. These prove quite effective in decreasing vibration attenuation.

In the industry, optimising for decreasing vibration attenuation can cause practical issues, most importantly an increase in noise amplification. Since the known PPF tuning methods are optimised for H_2 norms or H_∞ norms, these are based on pure disturbance transmissibility. This disregards the increase of the noise amplification, which can cause an increase of dynamic error of the performance. Noise amplification is usually considered by using *Dynamic Error*

Budgeting (DEB) to balance different disturbance and noise sources. DEB considers the total dynamic error that propagates through the system from these disturbances and this dynamic error is then minimised. This is often performed in Vibration Isolation systems [5, 6].

In this paper, a design approach for AVC on blade-like systems is presented, which accounts for the increase in noise transmissibility due to the controller gains. To achieve this, the effect of noise is analysed using DEB. PPF will be used as it is the most practical controller used with collocated piezoelectric patches. PPF tuning methods from literature are applied and a novel tuning is presented which accounts for the trade-off between disturbance rejection and noise amplification. Consequently, it is shown that by considering noise in the controller tuning, performance in terms of dynamic error can be increased. Finally, all results are experimentally validated.

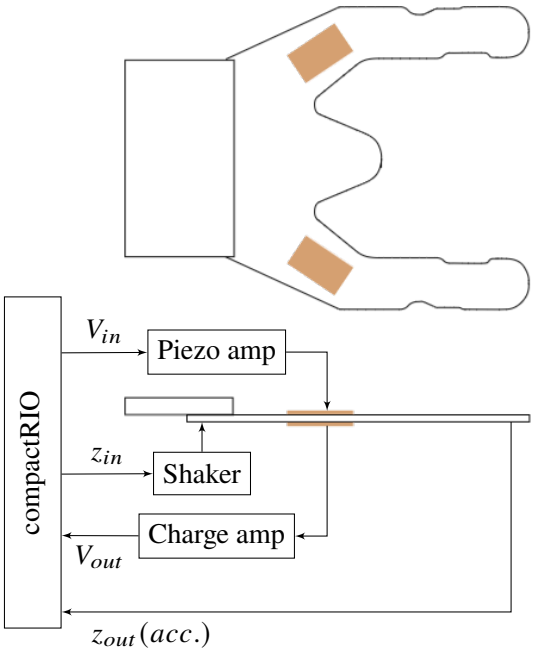

Figure 1. Inputs and outputs of the wafer handler gripper with AVC applied. Note that of V_{in},V_{out} and z_{out} there are 2 instances as there are 2 cantilevers or *prongs*. The piezo amplifiers used are the Piezoelectric Smart Materials HVA1500/50. The shaker is the Brüel & Kjael Shaker type 4809, driven by the shaker controller Brüel & Kjaer type 2706. The charge amplifiers are custom built with a lower frequency limit of around 4 Hz.

II. Problem definition

The problem presented in this paper is based on the Wafer Handler of the ASML Lithography machine. The company VDL Enabling Technologies Group B.V. is responsible for the design and production of the wafer handling system component of the machine. The purpose of the wafer handling system is to transfer silicon wafers from an atmospheric environment to the vacuum environment of the lithography machine, while conditioning it in temperature and position. The end-effector of the robot manipulator is a rigid and minimally damped structure composed of a thin ceramic plate. Because of docking contact between the robot manipulator and the wafer pick-up location, there are impulse disturbances. These disturbances are excite the bending modes of the cantilever end-effector, which can cause issues in pick-up accuracy of the manipulator.

To prevent this, Active Vibration Control is applied to the end-effector by bonding two pairs of collocated piezoelectric patches, actuator and sensor, to the surface. This setup is shown in Figure 1. This ultimately creates a 3-input (ground disturbance z_{in}, voltage inputs $V_{in,1}$ & $V_{in,2}$), 4-output (tip displacements $z_{out,1}$ & $z_{out,2}$, voltage outputs $V_{out,1}$ & $V_{out,2}$) MIMO system, defined as:

$$\begin{bmatrix} z_{out,1} \\ z_{out,2} \\ V_{out,1} \\ V_{out,2} \end{bmatrix} = \begin{bmatrix} P_{11} & P_{12} & P_{13} \\ P_{21} & P_{22} & P_{23} \\ P_{31} & P_{32} & P_{33} \\ P_{41} & P_{42} & P_{43} \end{bmatrix} \begin{bmatrix} z_{in} \\ V_{in,1} \\ V_{in,2} \end{bmatrix} \tag{1}$$

To describe the complete system, all 12 bode plots should be identified. However, there are many similarities between the two cantilevers of the end-effector. Both of the collocated piezoelectric pairs create a collocated Frequency Response Function (FRF) with alternating poles and zeros (P_{32} & P_{43}, Figure 2). The ground disturbance to tip displacements are the 2 performance FRFs (P_{11} & P_{21}, Figure 3). The cross terms P_{12}, P_{23} define how well the piezoelectric actuators can control the tip displacements, P_{31} and P_{41}

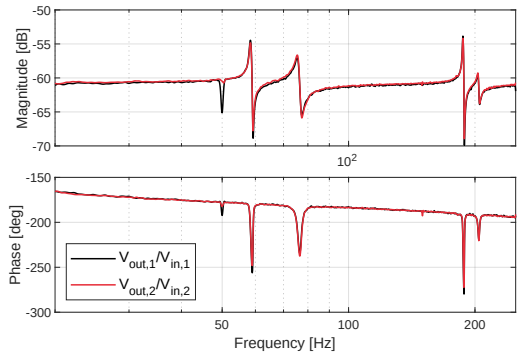

Figure 2. Collocated FRF $V_{out,1}/V_{in,1}$ and $V_{out,2}/V_{in,2}$

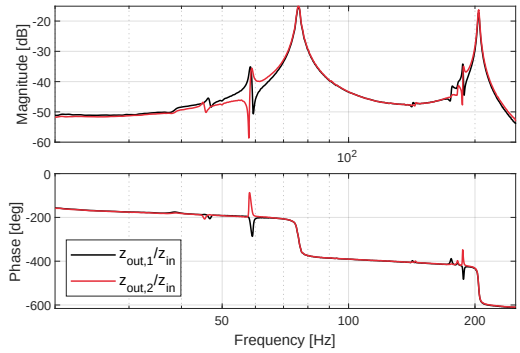

Figure 3. Performance channel FRF $z_{out,1}/z_{in}$ and $z_{out,2}/z_{in}$

define how well the sensors can sense the disturbance. The final cross terms P_{13} and P_{22} define the influence between the patch of one prong to the tip of the other prong. Figure 4 shows that the influence between the prongs is quite high, especially at the first mode around 58Hz.

A simpler system can be assumed where only 1 prong of the end-effector is considered, defining a 2x2 MIMO system as follows:

$$\begin{bmatrix} z_{out,1} \\ V_{out,1} \end{bmatrix} = \begin{bmatrix} G_{11} & G_{12} \\ G_{21} & G_{22} \end{bmatrix} \begin{bmatrix} z_{in} \\ V_{in,1} \end{bmatrix} \tag{2}$$

This simpler 2x2 system will be used to explain the general method that is introduced. The differences between the 4x3 system and 2x2 system are

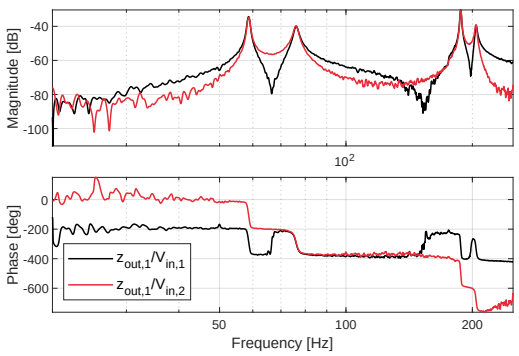

Figure 4. Prong *"communication"* cross term $z_{out,1}/V_{in,2}$ compared to $z_{out,1}/V_{in,1}$ shows that the piezo patch of the other prong has an equal effect around the poles as its own patch.

A. Defining performance

Since the goal of the Active Vibration Control system is to limit movement at z_{displ}, it can be stated that the total *variance of the dynamic error* e_z must be minimised. In this paper, this is achieved by using *Dynamic Error Budgeting (DEB)*. In this section, DEB is explained following [5]. For the calculations in this section, all disturbances and signals are assumed to be stochastic and zero-mean. For a zero-mean signal, the variance is equal to the power of the signal. In this paper, power means the mathematical definition of signal power, defined as:

$$\bar{x}^2 = \int_{-\infty}^{\infty} x(t)^2 dt \tag{3}$$

Also, all signals are assumed to be zero-mean, which means the variance of a signal is defined as $\sigma_x^2 = \bar{x}^2$. Now, the power of a signal is not evenly distributed. For stochastic signals, the power distribution over frequency can be modeled using the one-sided *Power Spectral Density (PSD)*, denoted with $S_x(f)$ and defined as the power of a signal over the frequency of a time signal $x(t)$. As the PSD is the distribution of power of the signal over the frequencies, the total area under the curve is equal to the total power or variance of the signal, defined as:

$$\sigma_x{}^2 = \int_0^{\infty} S_x(f) df \tag{4}$$

The *Cumulative Power Spectrum (CPS)* shows how different frequencies contribute to the total power of

the signal, defined by

$$C_x(f_0) = \int_0^{f_0} S_x(f)df \tag{5}$$

The value at $\lim_{f_0 \to \infty} C_x(f_0)$ will be σ_x. The CPS in an important tool to investigate the characteristics of the contributions of the signals and is used to compare these contributions easily.

As the total variance of the performance channel z_{displ} must be minimised, the PSD of the signal must be known. The influence of all contributions of all disturbance and noise sources can be defined as:

$$S_z(f) = \sum_{j=0}^{n} S_j {T_j}^2 \tag{6}$$

Here S_j defines the PSDs of n number of different input disturbances which can be ground vibrations, contact disturbances, electronic noise, or other inputs. T_j defines the FRF from that input source to the performance channel z. In many cases of Active Vibration Control, the largest biggest input is some kind of ground disturbance d with PSD $S_d(f)$, hence Eq. (6) is simplified as

$$S_z(f) \approx S_d {T_d}^2 \tag{7}$$

Since d is often a given and can not be controlled, T_d is then minimised. Methods such as H_2 and H_∞ control, which effectively minimise the magnitude of the performance FRF T_d. In practise, this simplification does not hold for many systems, where d is sufficiently small, or n, which defines electronic noise input, is sufficiently large.

The performance function as defined in Eq. (7) does not accurately define the performance as noise contributions become a significant part of the dynamic error. This can be the case for systems with small disturbances and higher precision, or systems with significant noise levels. To account for the noise contributions the following equation can be used:

$$S_z(f) \approx S_d {T_d}^2 + S_n {T_n}^2 \tag{8}$$

Finally, the total power or variance of the signal z can be calculated with

$$ {\sigma_z}^2 = \int_0^{\infty} S_z(f)df \tag{9}$$

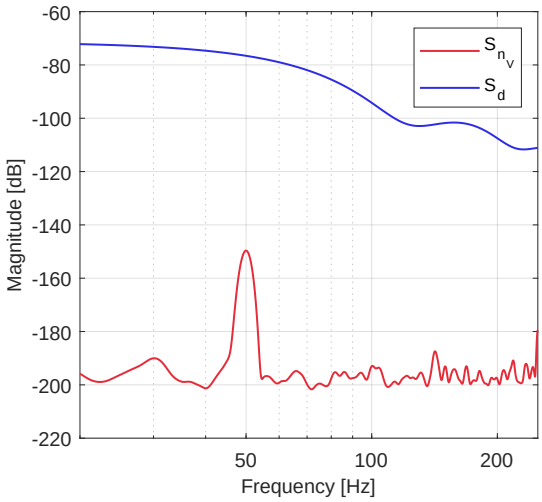

Figure 5. Power Spectral Densities of n_V and d. Calculated using the MATLAB® function *pwelch*

Inserting Eq. (8) into Eq. (9) gives the function that defines the performance of the active vibration controlled system as defined in the start of this Section. Eq. (8) shows the trade-off between the noise amplification $S_n {T_n}^2$ and the vibration attenuation $S_d {T_d}^2$.

Now, to solve this trade-off, the characteristics of the signals d, n_V and n_u must be known by calculating the PSD's of the signals, where d is the input z_{in} with impulses, n_V is the piezo output $V_{out,1}$ or $V_{out,2}$ measured with no inputs acting on the system, and n_u is the measured input $V_{in,1}$ or $V_{in,2}$ with no other inputs and without control. In the wafer handler system, n_u was disregarded because it was extremely small and difficult to measure. d is assumed to be 10x an impulse (physically defined as the top half of a sine wave, duration 20ms) with 3 seconds between each impulse. The calculated PSD of d and measured PSD of n_V are shown in Figure 5.

In the following section, the propagation from the disturbance and noise sources to the $z_{out,1}$ output is explained as the FRFs T_d, T_{n_u}, and T_{n_V} are defined.

III. Noise-disturbance propagation

To find the optimum of the trade-off introduced in the previous chapter, the propagation of the disturbance and noise sources must be known.

As an example, Figure 6 shows how different noise sources are introduced in the 2x2 MIMO model as

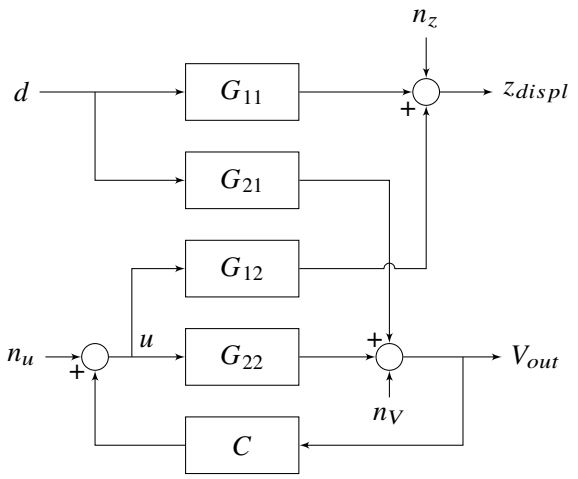

Figure 6. 2x2 MIMO decentralised control law including noise and cross-talk influences

defined in Section II. n_u is noise due to the piezo amplifier, n_z and n_V are sensor noises of the accelerometer and piezoelectric transducer respectively. How these noise sources propagate through the model to z_{displ} is defined by the following functions.

$$T_d = \frac{z_{displ}}{d} = G_{11} + G_{21}\frac{C}{1 - CG_{22}}G_{12} \tag{10}$$

$$T_{n_u} = \frac{z_{displ}}{n_u} = G_{12}\frac{1}{1 - CG_{22}} \tag{11}$$

$$T_{n_V} = \frac{z_{displ}}{n_V} = G_{12}\frac{C}{1 - CG_{22}} \tag{12}$$

$$T_{n_z} = \frac{z_{displ}}{n_z} = 1 \tag{13}$$

These equations define the FRFs between the noise source j and the output z_{displ}. Inserting these into Eq. (6) gives a total error estimate of

$$\sigma_z^2 = \int_0^\infty S_z(f)df \tag{14}$$

$$S_z(f) \approx S_d {T_d}^2 + S_{n_u} {T_{n_u}}^2 + S_{n_V} {T_{n_V}}^2 + S_{n_z} \tag{15}$$

In modelling the 4x3 MIMO system as described in Ch. II, the influence between the two cantilevers can not be neglected, as discussed in Section II. The formulas for T_d, T_{n_u}, T_{n_V} are more complicated for the 4x3 system, and are best calculated using

$$P_{cl} = C(1 + PC)^{-1} \tag{16}$$

Where P is the 4x3 plant matrix as defined by Eq. (1) and C is the 3x4 control matrix, defined by:

$$C = \begin{bmatrix} 0 & 0 & 0 & 0 \\ 0 & 0 & c & 0 \\ 0 & 0 & 0 & c \end{bmatrix} \tag{17}$$

Since both piezoelectric sensor cause a noise n_{V_1} and n_{V_2} they are both important to consider in the total equation for $S_{z,1}$. If these noise sources are assumed to be completely uncorrelated, the total influence of $n_{V,1+2}$ would be determined by

$${T_{n_{V,1+2}}}^2 = T_{n_{V,1}}^2 + T_{n_{V,1}}^2 \tag{18}$$

Which is using the pythagorean theorem to add the amplitude of two stochastic signals. However, this greatly overestimates the contribution of these two noise sources. Because $n_{V,1}$ and $n_{V,2}$ are both generated mostly due to the power supply of the charge amplifiers, the signals are actually correlated to a large degree. Hence, it will be assumed that the noise sources are equal and $n_{V,1} = n_{V,2} = n_V$. In the Appendix, this assumption will be clarified. Assuming the noise sources are equal, the influence of them is calculated with

$$\begin{aligned} {T_{n_V}}^2 &= (T_{n_{V,1}} + T_{n_{V,2}})^2 \\ &= (cP_{cl,12} + cP_{cl,13})^2 \end{aligned} \tag{19}$$

Using the symbolic math toolbox in MATLAB® to solve for P_{cl} and T_{n_V}, the following function is derived for T_{n_V} for the 4x3 system:

$$T_{n_V} = \frac{f(P,c)}{g(P,c)} \tag{20}$$

where

$$\begin{aligned} f(P,c) &= c^2\left(P_{13}P_{42} - P_{12}P_{33} - P_{13}P_{32} - P_{12}P_{43}\right) \\ &\quad + c\left(P_{12} + P_{13}\right) \\ g(P,c) &= P_{32}c + P_{43}c + P_{32}P_{43}c^2 - P_{33}P_{42}c^2 + 1 \end{aligned}$$

T_d for the 4x3 system is defined as follows:

$$T_d = \frac{f(P,c)}{g(P,c)} \tag{21}$$

where

$$\begin{aligned} f(P,c) &= P_{11} + c(P_{11}P_{32} - P_{12}P_{31} + P_{11}P_{43} - P_{13}P_{41}) \\ &\quad + c^2(P_{11}P_{32}P_{43} - P_{11}P_{33}P_{42} - P_{12}P_{31}P_{43} \\ &\quad + P_{12}P_{33}P_{41} + P_{13}P_{31}P_{42} - P_{13}P_{32}P_{41}) \\ g(P,c) &= P_{32}c + P_{43}c + P_{32}P_{43}c^2 - P_{33}P_{42}c^2 + 1 \end{aligned}$$

IV. PPF tuning optimisation

To tune the PPF for dampening the 78Hz mode, various methods can be used. For SISO systems, the PPF target frequency ω_c is set equal to the target mode frequency ω_n. But targeting the target mode in the MIMO case does not yield effective results. For MIMO cases, the PPF will be tuned to a different frequency in order to dampen the target mode. Using optimisation methods such as H_2 and H_∞, the tuning and other controller parameters are chosen. For the H_2 and H_∞ optimisation methods, the cost functions for a 2x2 cantilever system, where the closed-loop T_d is optimised, are defined as follows:

$$H_\infty = \max(|T_d(f)|) \tag{22}$$

$$H_2 = \int_0^\infty ||T_d(f)||^2 \mathrm{d}f \tag{23}$$

T_d is the closed-loop version of G_{11} as defined in Eq. (10.) These cost functions quickly become complicated for systems of higher orders. In [4], the analytical H_2 and H_∞ optimum for a 2x2 MIMO cantilever system with a single mode is derived.

A simpler possibility is by using a feed-through term on the plant, as introduced in [7]. This feed-through term effectively increases the distance between the pole and the zero in the collocated FRF, which, as explained in [2] and [8], increases possible reachable damping of the performance target mode. In this case, the PPF is tuned to the target mode. Less controller damping and higher gains will always increase damping, which simplifies the tuning.

The feed-through term can also be seen as a constant negative feedback on the controller, which modifies the effective controller that is consequently applied to the system. Performing this calculation on PPF, the effective controller is defined as:

$$C_{Ft} = \frac{C}{1 + FtC} = \frac{g}{\frac{s^2}{\omega_c^2} + 2\xi\frac{s}{\omega_c} + 1 + gFt} \tag{24}$$

Usually this feed-through term is chosen to be equal to the steady-state gain of the collocated plot, as this creates the largest pole-zero distance. A delta is added so the feed-through term comes just above this line, which helps with stability. This changes the equation to

$$C_{Ft} = \frac{g}{\frac{s^2}{\omega_c^2} + 2\xi\frac{s}{\omega_c} + 1 + g(G_{22}(0) + \delta)} \tag{25}$$

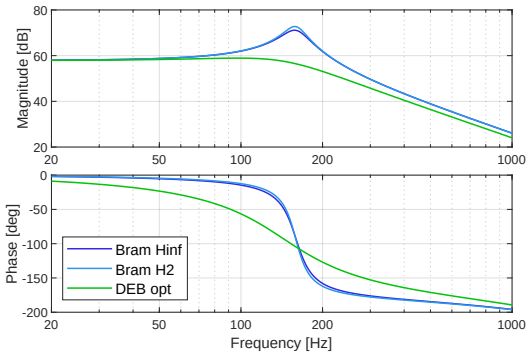

Figure 7. All PPF transfer functions for each optimisation with open loop gain $k = 0.7$.

As defined by [2], the stability condition of PPF is $C(0)G_{22}(0) < 1$. With the following equation it is shown that, for any g and $\delta \approx 0$, the feed-through PPF will be closed-loop stable.

$$C_{Ft}(0)G_{22}(0) = G_{22}(0)\frac{g}{1 + gG_{22}(0)} \tag{26}$$

$$\lim_{g\to\infty} C_{Ft}(0)G_{22}(0) = 1 \tag{27}$$

Which means that, for $\delta \approx 0$, $C_{Ft}(0)G_{22}(0)$ heads towards 1 asymptotically.

Generally, a gain margin is chosen, as practical phenomena like noise or identification errors can destabilise the system. This gives an open-loop gain k of $k = 1 - GM$. The controller gain value g can then be calculated with

$$g = \frac{k}{G_{22}(0) - k(G_{22}(0) + \delta)} \tag{28}$$

Three methods of PPF tuning are considered:

1) H_2 optimisation by [4]
2) H_∞ optimisation by [4]
3) Numerically minimised Dynamic Error with cost function Eq. (8) with $S_z(f) = S_d{T_d}^2 + S_{n_V}{T_{n_V}}^2$ with T_d and T_{n_V} as defined by Eq. (21) and (20). Because n_u is extremely small and n_z is constant, these are excluded from the cost function.

The multivariable numerical DEB optimisation is performed using the MATLAB® function *fmincon*, which is a nonlinear numeric optimising function. The target mode is the resonance mode at 78 Hz. Reason for this is because as seen in Figure 5, the

lower frequencies are attenuated more than higher frequencies due to the imperfect nature (top half of sine waves) of the impulse disturbances. A gain margin of $GM = 0.3$ is chosen which means $k = 0.7$ for all controllers. For the numerical optimisation, g is calculated at every step using Eq. (28). The two free variables of the optimisation are δ and ξ_c. Using the optimum PPF controllers, the closed-loop systems can be calculated using equation 16. MATLAB® enables numeric calculations of FRFs without parameter estimations by using Frequency-response data models *(frd)*. The closed-loop calculations are compared to the measured data in the following section.

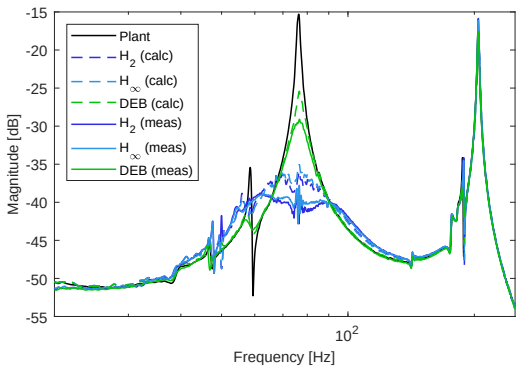

Figure 9. Measured closed loop FRFs $z_{displ,1}/z_{in}$

V. Results

First, the PPF transfer functions for the 3 different optimum controllers are shown in Figure 7. A significant difference is already observed as the DEB optimised controller has a higher controller damping ξ_c. Examining the closed-loop T_d FRFs in Figure 9, it is observed that the H_2 and H_∞ optimisations create considerably more damping of the target mode than the DEB-optimised method. The DEB optimised controller is a lot more conservative in damping the mode. By this performance metric, it would appear that the DEB optimised controller is not particularly effective. Figure 8, shows the result of every optimisation method in total dynamic error at z_{displ}. First, notice that the 78Hz mode has indeed the largest contribution to the total dynamic error in the uncontrolled plant, as expected. Second, it is clear that although the H_2 and H_∞ methods provide lots of disturbance rejection, they also introduce a lot of noise. In fact, the dynamic error due to the noise amplification is almost twice as much as the dynamic error due to the disturbance. Because the DEB-optimised controller is a lot more conservative in disturbance rejection, the dynamic error due to the noise is a lot less. The total dynamic error compared to the H_2 method decreases with 13% as the noise decreases with around 75%.

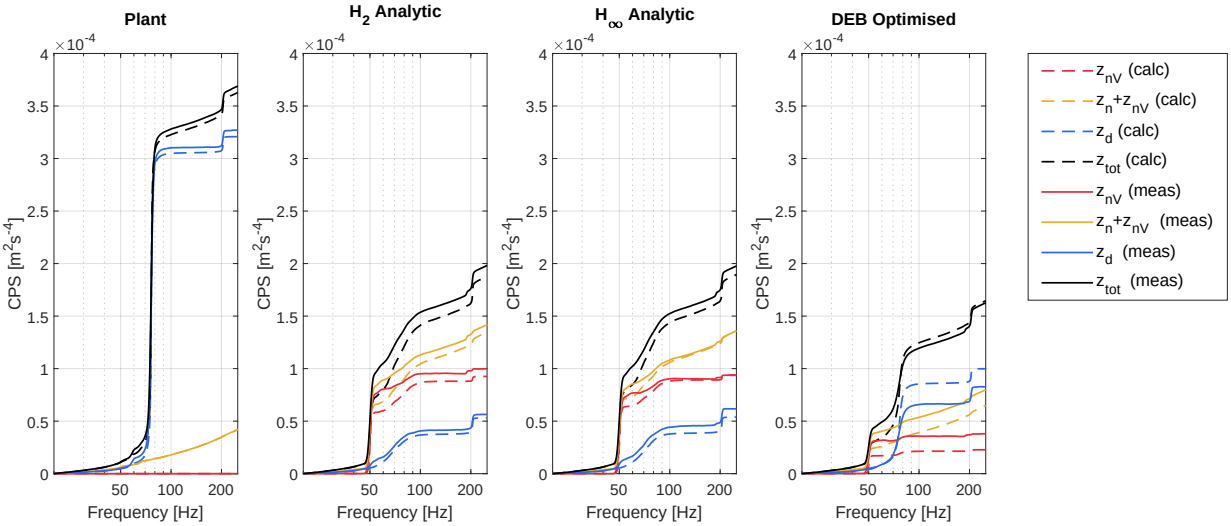

Figure 8. Cumulative Power Spectrums of different optimisation methods for PPF.

VI. Conclusion

This paper demonstrates how both the disturbance and electronic noise determines the performance of an Active Vibration Controlled system. The characteristics and propagation of the disturbance and electronic noise sources define the total dynamic error at the performance channel, defined by Eq. (6.) To optimise the damping performance, the dynamic error must be minimised. This means one must not only look at the propagation of the disturbance, but also at the propagation of the noise, as well as the characteristics of the disturbance and the noise.

The numerical DEB optimisation performed gives an example of a controller that optimises the trade-off between the disturbance and noise influence on the performance channel. The experimental results confirm the results of the calculations, and a clear improvement of performance can be observed.

Though the performance of Active Vibration Controlled systems is often defined as the performance FRF T_d, in reality, the objective is to decrease the dynamic error at a specific location such as the tip of a cantilever. In that sense, it does not matter if the dynamic error is caused by vibration attenuation or noise amplification. The results from this article provide a clear direction for mechatronic engineers to design an AVC system such that the total dynamic error is minimised.

Another advantage of decreasing noise amplification is that the amplified noise is in fact constantly present, which produces a constant dynamic error. Considering the constant dynamic error caused by noise helps in making the trade-off between noise amplification and disturbance rejection.

Acknowledgments

The author thanks Bram Seinhorst for his insights into the numeric calculations of the systems. Also, he thanks the group members of the MetaMech project at the TU Delft for their continuous insights and support during the project. Finally, he thanks Maurits van den Hurk and his colleagues at VDL E.T.G. for the support and insights in the wafer gripper system.

References

[1] Kim, S. M., Wang, S., and Brennan, M. J., "Dynamic analysis and optimal design of a passive and an active piezo-electrical dynamic vibration absorber," *Journal of Sound and Vibration*, Vol. 330, No. 4, 2011, pp. 603–614. doi: 10.1016/j.jsv.2010.09.004.

[2] Preumont, A., *Vibration control of active structures*, Vol. 4th, 2018.

[3] Paknejad, A., Zhao, G., Osée, M., Deraemaeker, A., Robert, F., and Collette, C., "A novel design of positive position feedback controller based on maximum damping and H2 optimization," *JVC/Journal of Vibration and Control*, Vol. 26, No. 15-16, 2020, pp. 1155–1164. doi: 10.1177/1077546319892755.

[4] Seinhorst, B., Nijenhuis, M., and Hakvoort, W., "H_\infty optimal positive position feedback for vibration control," *Book of Abstracts, 42nd Benelux Meeting on Systems and Control*, 2023, pp. 225–225. URL `https://www.beneluxmeeting.nl/2023/uploads/papers/boa.pdf`.

[5] Wouter Monkhorst, "Dynamic Error Budgeting a design approach," , 2004. URL `https://repository.tudelft.nl/islandora/object/uuid%3A073a04ec-6cb6-4e08-854f-8f063a7aaa44`.

[6] Jabben, L., and van Eijk, J., "Performance analysis and design of mechatronic system," *DEB Mikroniek*, Vol. 51, No. 2, 2011, pp. 5–12.

[7] Aphale, S. S., Fleming, A. J., and Reza Moheimani, S. O., "Integral resonant control of collocated smart structures," *Smart Materials and Structures*, Vol. 16, No. 2, 2007, pp. 439–446. doi: 10.1088/0964-1726/16/2/023.

[8] Piron, D., Pathak, S., Deraemaeker, A., and Collette, C., "On the link between pole-zero distance and maximum reachable damping in MIMO systems," *Mechanical Systems and Signal Processing*, Vol. 181, 2022. doi: 10.1016/j.ymssp.2022.109519.

Appendix: correlated noise sources

The transfer functions $\frac{z_{out,1}}{n_{V,1}}$ and $\frac{z_{out,1}}{n_{V,2}}$ define how either noise source at the location V_{out} propagates to the $z_{out,1}$ output. Figure 11, these two contributions are displayed.

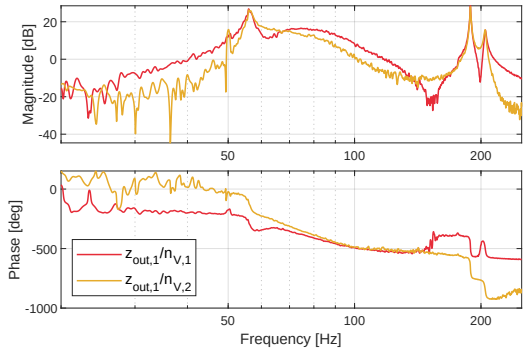

Figure 11. Two different n_V noise source contributions (closed loop for H_2), $\frac{z_{out,1}}{n_{V,1}}$ and $\frac{z_{out,1}}{n_{V,2}}$

Clearly, the contributions are almost equal. So, it is important to consider both noise sources for the total n_V noise contribution. For the total contribution of both noise sources, they must somehow be added together. For fully non-collocated signals, the amplitude of these contributions would add together according to the pythagorean theorem:

$$T_{n_{V,1+2}}{}^2 = T_{n_{V,1}}^2 + T_{n_{V,1}}^2 \qquad (29)$$

In Figure 10, the effect of this assumption is shown. A big overestimate of the noise is seen for the H_2 and H_∞ controllers, because these have a lot more noise contribution. Investigating the source of the noise $n_{V,1}$ and $n_{V,2}$, they can come from the following things:

- Piezoelectric patch sensor error
- Charge amplifier power supply noise or power grid noise
- Crosstalk between unshielded cables
- CompactRIO measurement error

Looking at Figure 5, it is clear that the noise consists of a 50Hz component and white noise. Since the 50Hz component suggests a power grid noise, it most likely comes from the power supply of the charge amplifiers. Because both charge amplifiers use the same power supply, this part of the noise can be assumed equal. As the 50Hz part of the noise is relatively large, the other parts of the of the noise sources are neglected and the complete noise sources $n_{V,1}$ and $n_{V,2}$ are assumed equal. By following this reasoning, the contributions of the noise sources can be added by summing up the transfer functions. This way, the 180° phase different is taken into account and the noises partly cancel. Hence Eq. (19) is used for the estimate of the contributions. As observed in Figure 8, this assumption is a lot closer to the real measured signal.

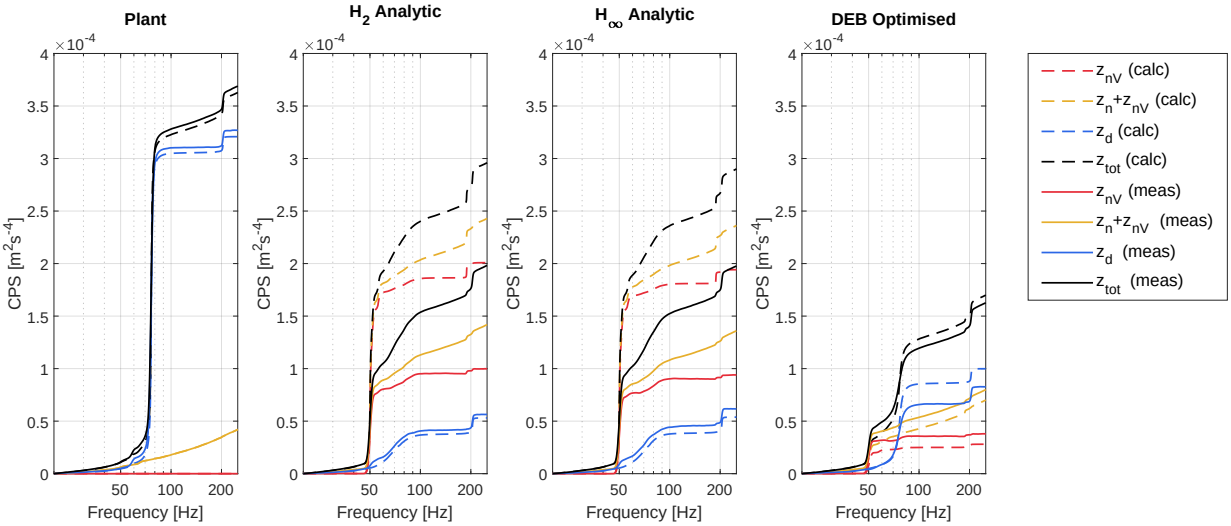

Figure 10. CPS, but the noise sources $n_{V,1}$ and $n_{V,2}$ are assumed to be non-corrolated

3

Conclusion & Discussion

This research aimed to answer the following research questions:

- How is performance defined in an Active Vibration Controlled system for a lightly damped, blade-like structure?
- What is an effective controller designed for optimising the performance of an Active Vibration Controlled system for a lightly damped, blade-like structure?

The research identified the performance as the total movement, or dynamic error, of the tip of the cantilevered system. Findings from the literature study show that Dynamic Error Budgeting can clearly show this performance in a plot of the Cumulative Power Spectrum. As this defines the total variance of each contribution to the error and the total error, it is a direct visualisation method of the performance of the vibration controlled system. Apart from a visualisation method of the performance, the CPS can be used as a cost function for a numerical optimisation. This way, it can be compared to other optimisation methods such as H_2 and H_∞. The results show a clear improvement in total dynamic error between the DEB-optimised controller and the traditional controllers.

An important limitation of the results is that its usefulness is specific to the system. In the wafer gripper system, optimising the noise-disturbance trade-off payed off in the case where the noise-disturbance ratio was big enough where the electronic noise would actually make a difference. For situations with larger disturbances or less noise, the optimisations make little to no difference.

The results show a clear improvement between the different cost functions of the optimisations. This should not come as a surprise, as the cost function of the performance metric is expected to be better than one that is not optimised for the same performance metric. The insight this study shows is how the performance of an AVC system should be defined. Many theoretical papers about AVC disregard noise. Reasons for this can be because noise is often a sufficiently small part of the system, because noise levels can be improved by choosing better equipment, or because it is often not the goal or purpose of a paper to show all practical implications that a physical AVC system will encounter. But as the precision, speed and accuracy of AVC systems will improve, the disturbances become smaller and smaller, it can be expected that the relative effect of noise becomes greater.

3.1. Future steps

The future steps are summed in two categories. First, originating from the noise-disturbance trade-off, future work may contain:

- **Analytical or mathematical optimum.** This study defines the performance as the trade-off in the dynamic error between the disturbance and noise, and this is numerically optimised. Though the results show the potential in the cost function, it is not certain a true optimum is reached, as numeric optimisation can encounter local optima and accuracy issues. A mathematical derivation can possibly be investigated to find a more global optimum for the problem.
- **Different optimisations** such as using different controllers or a simpler optimisation might be possible to give more insights into the results. Varying open-loop gain instead of other parameters could possibly give better results.

Second, from the VDL wafer gripper perspective, there are several possible research directions that follow from this study:

- **Damping of multiple modes.** The second resonance was disregarded in this research but it clearly has an influence on the total dynamic error. Because the disturbance was estimated with the top half of a sine wave with a specific length, the first resonance was attenuated a lot more than the higher frequency modes, due to the shape of the PSD of the disturbance. Modelling the disturbance in a different way could mean that the higher frequency modes are attenuated more, and damping could be necessary on those modes.
- **Placement of the piezoelectric patches.** The placement was done in the previous work of [9] using a simple line optimisation to achieve high observability and controllability of the first mode. As was suggested in the literature study in Appendix A.5, a near-collocated setup of the piezoelectric patches could result in a larger pole-zero distance, which is essential to improve damping performance and is the same reason why feed-through increases performance. Further research on patch placement, orientation and near-collocation could give possible performance benefits.

Finally, as the wafer gripper has been investigated on the current free-free setup and shown sufficient results, the next step for the industry is to apply it on the actual machine. Practical considerations in the design such as the thickness the piezoelectric patch add must be reconsidered. As the wafer gripper is mounted on a SCARA manipulator arm, the vibration attenuation can be expected to be even greater than it is now due to the bigger cantilever. Also, the actual disturbance and noise spectra will require different tuning and possibly require tuning of multiple modes.

References

[1] Sang Myeong Kim, Semyung Wang, and Michael J. Brennan. “Dynamic analysis and optimal design of a passive and an active piezo-electrical dynamic vibration absorber”. In: *Journal of Sound and Vibration* 330.4 (Feb. 2011), pp. 603–614. ISSN: 0022460X. DOI: 10.1016/j.jsv.2010.09.004.

[2] Mark J. Balas. “Direct Velocity Feedback Control of Large Space Structures”. In: *Journal of Guidance and Control* 2.3 (May 1979), pp. 252–253. ISSN: 0162-3192. DOI: 10.2514/3.55869.

[3] A Preumont. *Mechatronics Dynamics of Electromechanical and Piezoelectric Systems*. Vol. 136. 2006. ISBN: 1-4020-4695-2.

[4] André Preumont. *Vibration control of active structures*. Vol. 4th. 2018.

[5] Dimitri Piron et al. “On the link between pole-zero distance and maximum reachable damping in MIMO systems”. In: *Mechanical Systems and Signal Processing* 181 (Dec. 2022). ISSN: 10961216. DOI: 10.1016/j.ymssp.2022.109519.

[6] Sumeet S. Aphale, Andrew J. Fleming, and S. O. Reza Moheimani. “Integral resonant control of collocated smart structures”. In: *Smart Materials and Structures* 16.2 (Apr. 2007), pp. 439–446. ISSN: 09641726. DOI: 10.1088/0964-1726/16/2/023.

[7] Wouter Monkhorst. *Dynamic Error Budgeting a design approach*. 2004. URL: https://repository.tudelft.nl/islandora/object/uuid%3A073a04ec-6cb6-4e08-854f-8f063a7aaa44.

[8] Leon Jabben and Jan van Eijk. “Performance analysis and design of mechatronic system”. In: *DEB Mikroniek* 51.2 (2011), pp. 5–12.

[9] Manal El Ajjaj. *Vibration suppression of a state-of-the-art wafer gripper*. 2022. URL: https://repository.tudelft.nl/islandora/object/uuid%3A671bba53-1a84-4c64-9d3b-ef4319f0e1c1.

A

Measurement setup and experiments

The VDL wafer gripper had to be extensively identified for all the range of results. In this appendix, all parts of the the measurement setup will be explained thoroughly.

A.1. Original setup

The wafer gripper was hanging in a free-free setup (Fig. A.1). This setup was originally designed by [9]. Piezo patches were placed as shown in Fig. A.2. The base disturbance was performed with a Brüel & Kjael Shaker type 4809, driven by the shaker controller Brüel & Kjaer type 2706. Originally, the measurements were done with the Polytec Scanning Vibrometer PSC-400. This machine can iterate over the surface and show mode shapes, as was performed in [9].

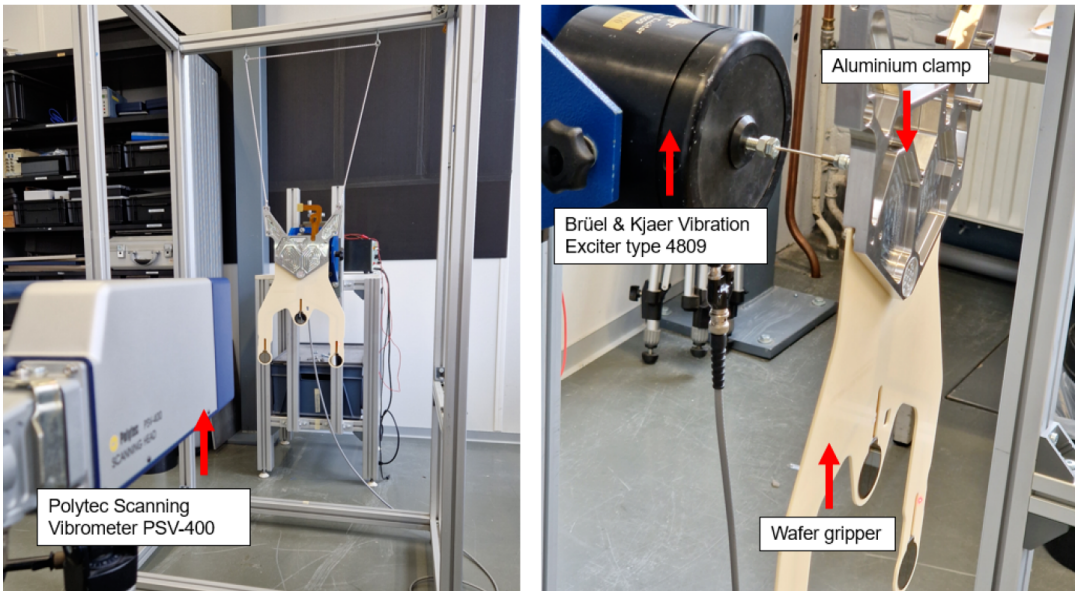

Figure A.1: Free-free hanging setup

To make the measurements simpler and more consistent, accelerometers were placed on the tips of the cantilevers. These would provide tip acceleration measurements. Further, the accelerometers used are extremely lightweight and thus don't significantly effect the system.

A.2. CompactRIO and Labview

To record all measurements, a CompactRIO-9039 with the following submodules was used:

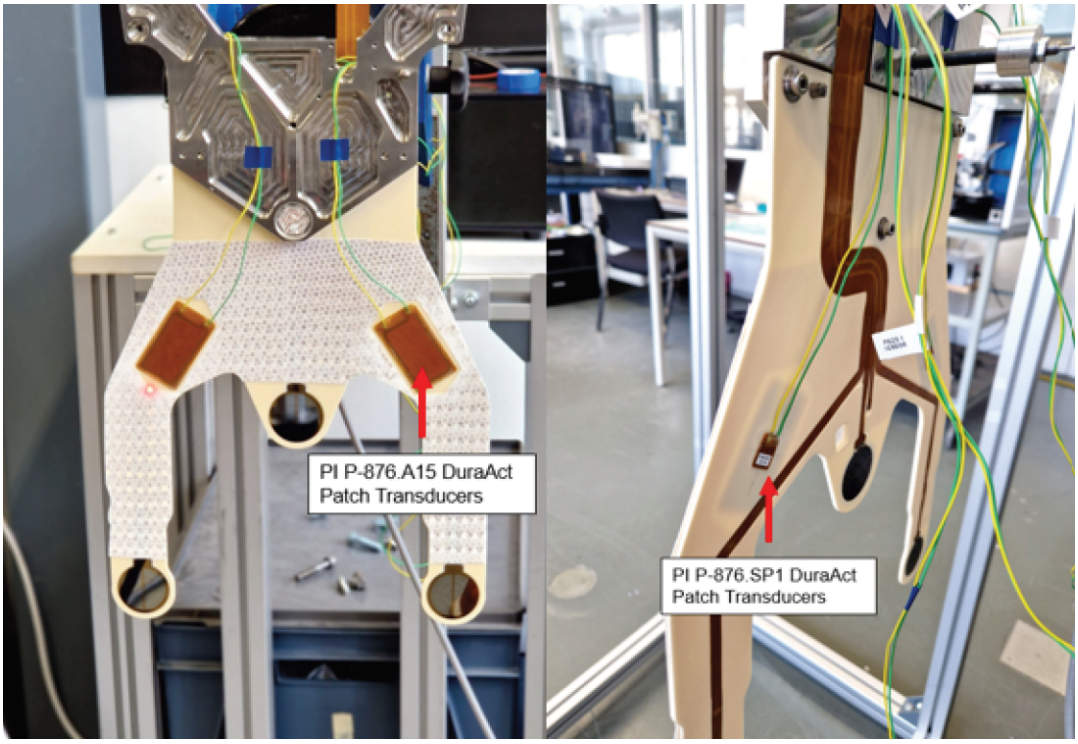

Figure A.2: Piezo patches configuration

1. NI 9201 Analog Input +- 10V 12 bit resolution
2. NI 9264 Analog Output +- 10V, 16 bit resolution
3. NI 9215 Analog Input +- 10V, 16 bit resolution
4. NI 9215 Analog Input +- 10V, 16 bit resolution

Initially, only module 1 and 2 were used. Though the 12-bit resolution of Module 1 created extra noise in the system, which is why Module 3 and 4 were added in a later stage. As these only had 4 inputs, 2 modules had to be used to replace module 1. The cRIO-9039 has an FPGA module that can be programmed for the measurements and control. As the gate arrays are physically programmed, this creates a very fast controller and measurement device. The FPGA ran at 10 kHz.

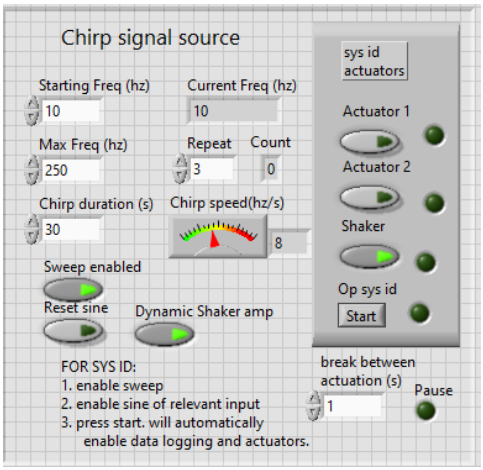

Figure A.3: Chirp signal instrument

Using the built-in computer of the cRIO, the FPGA could be handled as a Real-time module, and

information was passed to the FPGA module. All the different types of measurements could be completed automatically using the cRIO virtual instrument, including:

- Chirp signal (Fig. A.3).
  Perform a chirp signal with start and end frequency to a specific input. The program can switch automatically from each input to the next with a small pause inbetween. This way, the complete system identification can be performed automatically. Most of the measurements used a 30 second chirp from 20 to 250 Hz, repeated 3 times. Over 3 inputs, with a pause of 1 second between each input, this means one system identification would take exactly 272 seconds.
- Impulses (Fig. A.4)
  An impulse to the shaker input could be performed by pressing a single button. The impulse is shaped as the top half of a sine wave, with a pulse length of around 20 ms.
- Multiple impulses (Fig. A.4)
  To create a consistent disturbance, multiple impulses could be performed automatically. The disturbances are 10x impulses of 20ms width, with a time of 3 seconds between each pulse. This means that the total measurement time took 30 seconds.
- Measurements without impulses (Fig. A.4)
  To measure the noise levels of the system (with or without controller), a measurements of fixed time could be performed without any inputs. Since the impulses took 30 seconds, the noise measurement was 30 seconds aswell.

A.2.1. Dynamic shaker amplitude level

The shaker level input could be dynamically altered. Between the shaker and the base accelerometer, some modes existed (due to the shaker's coils). These modes could cause excessive vibrations which caused the accelerometers to overrange. The transfer function between the shaker input and the base accelerometer output was inverted and applied to the input of the shaker. This meant that the maximum amplitude of the shaker could stay high over most of the measurement, and the amplitude decreased around the shaker's eigenmodes. This was only done for the chirp signal measurements, as the transfer function calculations will automatically take into account the lower input, so nothing changes in the final transfer function (except that the entire transfer function will be less noisy because the inputs are generally higher).

A.3. Outputs (measurements)

The outputs of the system are as follows:

1. Piezoelectric sensor patch 1 (right) (PI P-876.SP1 DuraAct Patch Transducer)
2. Piezoelectric sensor patch 2 (left) (PI P-876.SP1 DuraAct Patch Transducer)
3. Accelerometer tip 1 (right) (SparkFun ADXL337)

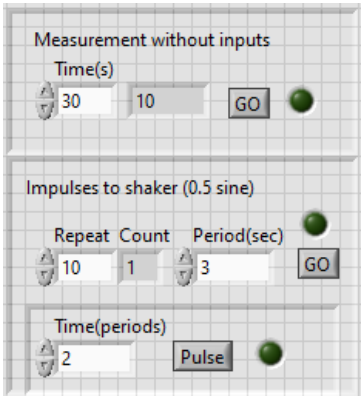

Figure A.4: Impulses and noise measurements instrument

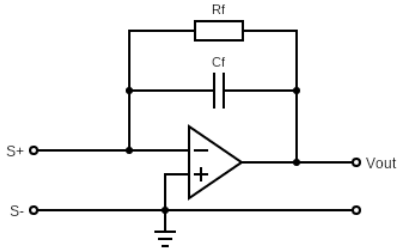

Figure A.5: Charge amplifier circuit. Values used are $Rf = 640k\Omega$ and $Cf = .082\mu F$

4. Accelerometer tip 2 (left) (SparkFun ADXL337)
5. Accelerometer base (SparkFun ADXL337)
6. Vibrometer input (tip 1 or 2)

The accelerometers and vibrometer could be connected directly to the cRIO for measurements. The vibrometer was only used for verification of the accelerometers, as the measurement were significantly slower using the vibrometer, as it could only target a single tip of the gripper at a time. The accelerometers provided constant measurements of both tips.

The base accelerometer was supposed to provide extra information about the base disturbance input. The transfer function between the disturbance input and the base accelerometer was used for the ”dynamic shaker level” (Sec. A.2.1)

A.3.1. Charge amplifier

The piezoelectric patches require a charge amplifier to create a well-defined flat steady-state response, as the piezoelectric measurements have a natural high-pass behaviour. The charge amplifier circuit is shown in Fig. A.5. The charge amplifier creates a pass-band behaviour. By choosing the input resistance very high, the low-pass is pushed toward a very high frequency. The high-pass cut-off frequency, or the lower frequency limit, is calculated with

$$f_l = \frac{1}{2\pi RfCf}$$

.

The high-pass cut-off frequency was chosen to be above 2.5 Hz. This value actually suppressed a low-frequency mode which exists because of the hanging free-free setup. The wafer gripper, hanging on the jump rope, created a pendulum with an eigenfrequency of around 2.5 Hz. This mode destabilized the PPF, since PPF has no low-frequency roll-off. The resistor value of $640k\Omega$ actually makes the charge amplifier’s high-pass cut-off frequency around 3 Hz, which suppresses the 2.5Hz mode. The result of the improved charge amplifier can be seen in Figure A.6.

A.4. Inputs (actuators)

The inputs of the system are as follows:

1. Base disturbance, Brüel & Kjael Shaker type 4809, driven by the shaker controller Brüel & Kjaer type 2706
2. Piezoelectric actuator 1 (right), PI P-876.A15 DuraAct Patch Transducers
3. Piezoelectric actuator 2 (left), PI P-876.A15 DuraAct Patch Transducers

The shaker could simply be driven by the accompanied shaker controller, directly connected to the cRIO analog output. An amplification level could be chosen on the shaker controller. It it important that between measurements, the amplification level would stay equal. For each measurements the used amplification level was recorded and noted.

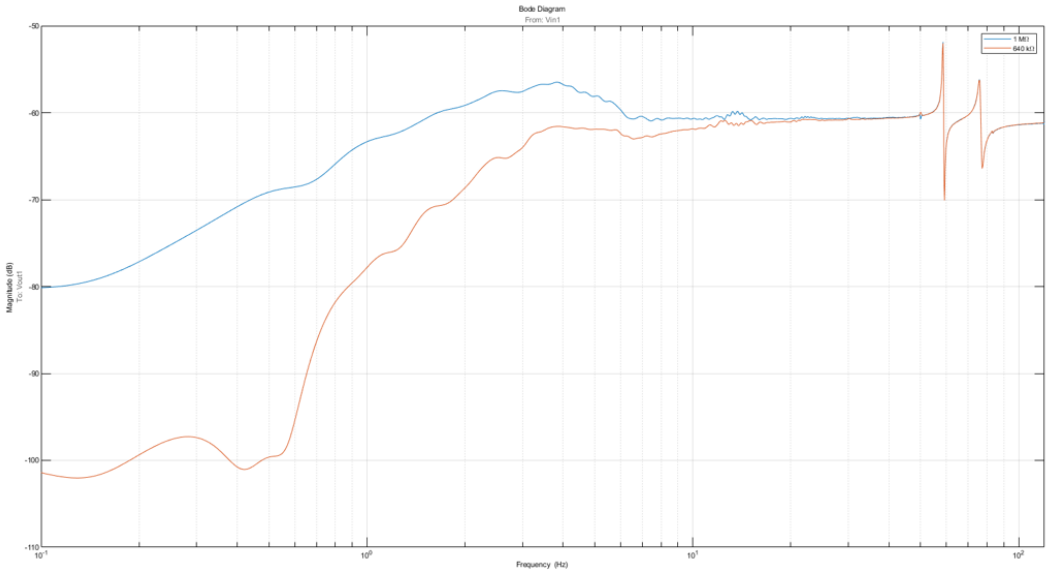

Figure A.6: Charge amp Rf values of $1M\Omega$ (blue) and $640k\Omega$ (orange)

The piezoelectric actuators require an amplifier to work. Originally, PiezoDrive BD300 dual channel amplifiers were used. Unfortunately, these amplifiers add a lot of noise, which could be constantly heard in the system. So, at last, Smart Material's HVA1500/50 Piezo amplifiers were used, which provide a much lower noise level.

A.5. Measurements documentation

To record all measurement and keep them organised, a single excel file was used, which include all information about the measurements' conditions and results, including:

For the DEB measurements

- Date
- Time
- Filename
- Charge amp resistance (for tracking measurements before and after the changed charge amplifier resistance)
- Input resolution (for tracking measurements before and after the improved AI module)
- Pzt amp (for tracking measurements before and after changing out the Piezoelectric amplifier)
- Duration of measurement
- Freq. start
- Freq. end
- Shaker lvl (making sure all measurements use the same Shaker controller's levels)
- Duration of impulses (ms)
- Period between impulses
- Number of impulses
- Controller type
- Controler gain (open loop or absolute)
- other controller information

For the system identification measurements

- Date
- Time
- Filename
- Charge amp resistance (for tracking measurements before and after the changed charge amplifier resistance)
- Input resolution (for tracking measurements before and after the improved AI module)
- Pzt amp (for tracking measurements before and after changing out the Piezoelectric amplifier)
- Freq. start
- Freq. end
- Shaker lvl (making sure all measurements use the same Shaker controller's levels)
- Use of the "dynamic shaker lvl"
- Duration of impulses (ms)
- Period between impulses
- Number of impulses
- Controller type
- Controler gain (open loop or absolute)
- other controller information

Literature Survey

Techniques for the mechanical and controller design of an active vibration controlled system: a technical review

by

Castor Verhoog

Student number: 4676491
Project duration: October 10, 2022 – July 21, 2023
Supervisors: Prof. dr. ir. H. HosseinNia TU Delft
ir. M. Kaczmarek, TU Delft, supervisor
ir. M. van den Hurk VDL ETG B.V.

TU Delft

Contents

Nomenclature

Abbreviations

Abbreviation	Definition
AVC	Active Vibration Control
CPS	Cumulative Power Spectral Density
DEB	Dynamic Error Budgeting
DVF	Direct Velocity Feedback
FRF	Frequency Response Function
HAC	High Authority Control
IRC	Integral Resonant Control
LAC	Low Authority Control
NDF	Negative Derivative Feedback
NPF	Negative Positional Feedback
PPF	Positive Positional Feedback
PSD	Power Spectral Density
SA	Sensor-Actuator

1 Introduction

Vibrations can arise in mechanical systems due to several factors, including external disturbances, unbalanced forces, or the inherent dynamics of the system design. This is particularly true for highly dynamic systems, such as in robotics or motion systems, where the motion and interactions of different components can generate unwanted vibrations. With the increasing performance demands of such dynamic systems, motions and accelerations increase, which also increases induced vibrations. These vibrations can cause accuracy problems and decreased performance.

Since these vibrations can decrease the performance of the system, engineers can design systems to increase damping of these vibrations. Traditionally, these systems are passive, such as Tuned Mass Damping, which is famously used in the tallest building in Taiwan, Taipei 101[1]. While passive damping methods such as Tuned Mass Damping and Constrained Layer Damping provide sustainable and electronics-free solutions to damping vibrations, they suffer from limited performance[2] and technological drawbacks. Tuned mass damping and constrained layer damping generally consume relatively much design volume to achieve acceptable performance, which can be a problem when the overall design volume is limited. Also, these systems have to be tuned and well integrated. If the system changes after this integration, for example because a robot manipulator increases in mass, the passive system is unable to account for the changes. These drawbacks also mean that it is difficult to implement them in existing systems. To overcome these problems, Active Vibration Control (AVC) has emerged as an alternative technology.

AVC utilises sensors and actuators with a control system to dampen the system's eigenmodes. Since the control system is software-based, active methods can be highly adaptive. They can be implemented in existing systems without complete system redesigns or drastic design changes, and can potentially adapt to changes in the system in real-time if required. These advantages make AVC methods highly popular in high-performance dynamic systems. Therefore, AVC has already been used in many examples, namely the semiconductor industry (motion systems), robotics (flexible manipulators), aerospace industry (wing vibrations), automotive industry (active suspension), and civil engineering (bridges)[1, 3–6].

Although AVC has been extensively discussed in papers and books [7–12], recent years have seen significant advances in the field. By utilising various optimisation methods and techniques, the performance of active vibration control systems can be significantly enhanced. With numerous possible systems available, there exist multiple controllers and techniques to improve performance for a given system. However, the performance of the AVC system is often indicated with varying performance metrics in different papers, making it difficult to compare the performance of different techniques. This lack of an overview makes it difficult for designers to design active damping systems in line with all recent developments.

In this view, this literature study aims to summarise and compare different techniques which designers can use to try and optimise active damping systems. The final result will be an extensive comparison of techniques which designers can use to design an active vibration controlled system for multiple purposes. The results of this literature study will consequently be applied to a relevant case study of the semiconductor industry. In the following section, the case study and its relevance will be explained further.

1.1. Case Study

In the semiconductor industry, performance demand has increased greatly. Semiconductors are found in every personal electronic device and as quality of life increases worldwide, demand for these devices and their performance increase is increasing. This means machines that manufacture semiconductors will have to increase its performance and precision to keep up with demand. ASML N.V. provides the world with lithography machines that make the semiconductor industry possible. These room-sized machines create the raw silicon chips found in every device. In addition to lithography, the machine handles silicon wafers with great precision and speed. VDL ETG B.V. designs and manufactures the wafer handling system part of the machine. The wafer handling system is designed to move silicon wafers from an atmospheric environment to the vacuum environment of the lithography machine through an airlock or vacuum vessel. The first system moves the wafers from the atmospheric pick-up spot to the vacuum vessel and a second system moves them from the vacuum vessel into the machine. The vacuum vessel includes a wafer prealigner, which aligns the wafer to a known position. The robot manipulator then docks with the prealigner, picks up the wafer, and moves the wafer onto the wafer stage. The robot manipulator end-effector is shown in Figure 1.1. The end-effector is a thin ceramic plate, which is a stiff, lightly damped structure.

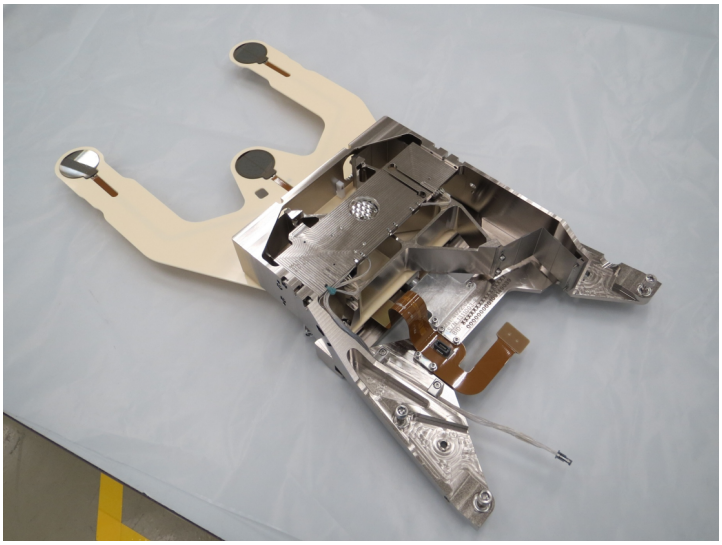

Figure 1.1: The robot manipulator's end-effector, which picks up the silicon wafers from the pre-aligner inside the vacuum vessel/airlock.

With docking between the robot manipulator and pre-aligner, the docking impact induces vibrations in the lightly-damped end-effector. While the end-effector is moving due to these vibrations, the wafer cannot be picked up as there is a risk of the wafer shifting and reduced pick-up accuracy. Because of this, the machine has to either wait for vibrations to settle before the wafer can be picked up or decrease its movement speed entirely to decrease the docking impact. This waiting time limits the total throughput of the machine. Increasing end-effector damping would reduce the settling time and thus increase the machine's throughput.

1.2. Previous work and initial problem investigation

This thesis continues the work of M. El Ajjaj [13] from September 2021 to July 2022. The use of AVC was investigated and compared to the use of passive or semi-passive methods such as constrained layer damping, tuned mass damper, or piezoelectric shunting. The thesis of M. El Ajjaj finished with a proof of concept in which Positive Positional Feedback (PPF) was used as controller and a maximum modal damping of the largest mode of 3.3% was reached. Higher gains resulted in an unstable system. This instability could not be explained as its open-loop steady-state gain did not increase above 1, which is defined as the PPF stability condition [7]. The first step in solving the case study was explaining the instability of the system for PPF gains greater than 0.5. To do this, the system dynamics must be thoroughly identified.

In order to describe the system's dynamics, an extensive system identification was performed. The system is a Multi-Input Multi-Output (MIMO) system, with 3 inputs: the ground vibration source and 2x piezoelectric actuators, and 4 outputs: 2x piezoelectric sensors and 2x tip displacements. With 3 inputs and 4 outputs, the system can be described with 12 bode plots. Using a combination of a Polytec Scanning Doppler Vibrometer PSV-400 and a TI Delfino Launchpad F2837XD, these bode plots were generated. Investigating the bode plots of the collocated transfer functions between the piezoelectric actuator and the sensor patches, the problem is quickly observed. The collocated bode plots show an absolute steady-state gain of 2. This means that the open-loop transfer with a PPF controller of 0.5 already reaches a steady-state gain of 1. This means that increasing the PPF gain further will destabilise the system, as observed by M. El Ajjaj in her thesis. Thus, as the instability is explained, the next step is to investigate how to increase the performance of the total system. In the thesis, the problem investigation is explained more extensively. Using the preliminary problem investigation, a literature research direction is chosen, which will be explained in the following Section.

1.3. Outline

To increase the performance of the case study AVC system, a different control approach must be selected. To select the correct approach, a literature study is performed. The goal of this literature study is to form a basis comparison of AVC techniques, to be used by any engineer who wishes to apply AVC to a stiff and lightly damped structure using (collocated) piezoelectric patches. In the literature study, the following questions will be answered:

1. What are suitable active vibration control techniques used for lightly damped structures?
2. How can the performance of different active vibration control techniques be compared and evaluated for lightly damped structures in terms of metrics such as vibration reduction and robustness?
3. How do the performance of different active vibration control techniques compare for lightly damped structures in terms of metrics such as vibration reduction and robustness?

First, an example problem is defined in Chapter 2. This example is used throughout the study and is used to show the effects of different mechanical design choices and controller designs, explained in Chapters 3 and 4. Finally, in Chapter 5, different performance metrics and objectives are defined. These can be used to compare the performance of the AVC techniques and consequently optimise the system. In Chapter 6 a final overview of the techniques will be shown and the research questions will be answered using the content of this study. In addition, a research plan for the thesis is presented.

Using the literature study, the appropriate approach can be selected for the case study. In the thesis, a hypothesis will be formed for the performance of the selected approach. The hypothesis will then be tested experimentally. The thesis research plan will be presented at the end of Chapter 6.

2 Problem Definition

This Chapter defines a common example problem that is used to illustrate the effects and properties of the various AVC techniques discussed in subsequent chapters. This problem is frequently used in AVC papers and should be comparable to real-world examples of AVC.

It is common for an AVC system to not be isolated from the ground, or the disturbance comes from somewhere near or within the system. Because of this, it is not possible to completely eliminate ground disturbances using Active Vibration Isolation techniques, such as feedforward control [7]. The assumption for the problem in this study is that it is impossible to detect ground disturbances before they have affected the system.

We define a cantilever with an input for ground disturbance and an output for tip displacement. The ground disturbance is amplified as it is transferred through the cantilever beam due to the beam's eigenmodes. This naturally causes peaks in the transfer function of z_{inp} to z_{displ}. This is illustrated in Fig. 2.1. As described in Chapter 1, excessive amplifications of these vibrations can result in a number of issues.

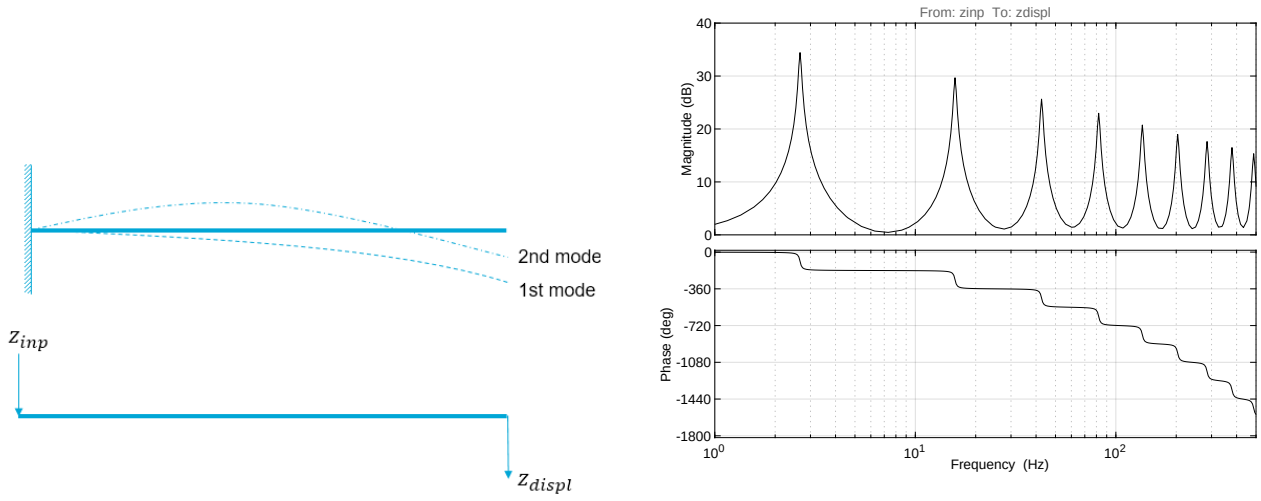

(a) System definition

(b) FRF ground disturbance to tip displacement

Figure 2.1: Simple cantilever system with ground vibrations input z_{inp} and tip displacement output z_{displ}

A sensor and actuator are added to the system in order to implement Active Vibration Control and reduce these amplifications. The control loop will be applied to this sensor-actuator (SA) pair. In AVC of lightly damped structures, piezoelectric patches are frequently used as sensors and actuators. Piezoelectric patches have a high internal stiffness that has no effect on the cantilever beam's lower frequency modes. In addition, the high internal stiffness permits high frequency control.

The location of the sensor and actuator will define the level of observability and controllability of each mode. Placing the sensor at a location with zero strain of certain mode shapes means that this mode will be unobservable, and placing an actuator at such a location means the mode will be uncontrollable.

If we place the sensor and actuator at the same location on the beam, the sensor actuator pair is collocated. This causes the observability of each mode to be equal to the controllability of that mode [7].

Observing the collocated system depicted in Figure 2.2, alternating resonances (poles) and anti-resonances (transmission zeros) are observed. This ensures that the phase remains between 0 and -180 degrees, providing high-frequency stability for a range of controllers.

(a) System definition. V_{top} is the actuator, V_{btm} is the sensor

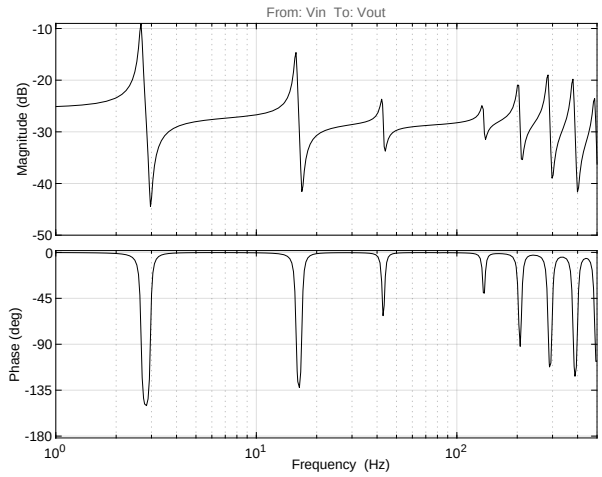

(b) Bode plot $\frac{V_{btm}}{V_{top}}$. The bode plot shows the alternating poles and zeros, which guarantee the phase to be between 180 and -180 degrees

Figure 2.2: Cantilever system with a collocated piezoelectric sensor-actuator pair, input V_{top}, output V_{btm}

The total system will include 2 inputs (z_{inp} and V_{in}) and 2 outputs (z_{displ} and V_{out}), which makes it a MIMO system. The transfer function $\frac{z_{displ}}{z_{inp}}$ defines the objective of the active vibration control, as the goal is to limit the tip displacement. The transfer $\frac{V_{out}}{V_{in}}$ is where the feedback loop is applied to, as these are the input and output voltages of the piezoelectric sensor and actuator patches. This means the controller is a decentralised SISO controller. The transfers $\frac{V_{out}}{z_{inp}}$ and $\frac{z_{displ}}{V_{in}}$ are defined as the cross-talk terms[7]. These are defined by the mechanical and controller design choices and show how well the controller actually controls the objective function z_{displ}/z_{inp}.

In the rest of this literature study, the example explained in this chapter is used as model to show the effect and workings of each technique on the system. As explained, the example is a MIMO system with a SISO controller. The actuator and sensor placement is assumed to be collocated or at least nearly-collocated, which will be further explained in the following Chapter.

3 Mechanical Design

Although the majority of literature is focused on designing the control law for AVC, the mechanical design of the AVC system poses various possibilities for optimising the performance of such a system. In [14], a detailed technical review of the following well-researched optimisation criteria is performed: (i) maximising modal forces/moments applied by piezoelectric structures, (ii) maximising deflection of host structure, (iii) minimising control effort/maximising energy dissipated, (iv) maximising degree of controllability, (v) maximising degree of observability, and (vi) minimising spillover effects. From this study, it is abundantly clear that the result of the location optimisation study is highly dependent on the criteria used. [15] introduces the use of observability and controllability Grammians as performance indices, which use multiple of these criteria. This technique has been shown to work in multiple examples [16–19].

Furthermore, many different algorithms have been used for these optimisation criteria, such as a spatial H_2 norm [20] and genetic algorithms [18, 21]. All these optimisation techniques are focused on open-loop optimisation, which means they do not consider added dynamics by the controller. Since these dynamics can play significant roles in closed-loop, focusing the SA optimisation on open-loop only can lead to sub-optimal solutions, as presented by [22].

This problem can be solved by optimising SA placement with a closed-loop performance index, such as modal damping, as an example performed in [23]. Closed-loop optimisations, while computationally heavy, can provide solutions for engineers to optimise SA placement for complete systems. Generally, the complete system must be optimised for each SA location. That is, the controller parameters have to be optimised for each location, as the optimal parameters are different per plant. As different controllers with their corresponding optimisation methods are explained in Chapter 4, performance indices for closed-loop mechanical optimisation for SA placement are discussed in 5.

Because most open-loop optimisation techniques have been extensively reviewed, these techniques will not be discussed and the reader is referred to Gupta et al.[14]. This Chapter does not provide an extensive comparison of these techniques, but rather introduces a technique not reviewed by Gupta et al, which is the pole-zero distance.

3.1. Electromechanical coupling factor

As defined by Preumont in [7], electromechanical coupling factor K_i defines a measure of the efficiency of the conversion of electrical energy to mechanical energy (strain), and vice versa. It is generally experimentally determined, by measuring the natural frequency of the system with open-loop electrodes Ω_i and closed-loop electrodes ω_i, and can then be calculated using

$$ {K_i}^2 \approx \frac{{\Omega_i}^2 - {\omega_i}^2}{{\omega_i}^2} \tag{3.1} $$

It can also be calculated analytically using the admittance of the beam. This is extensively explained and performed in [13]. Optimisations for SA placements for cantilever beams, using the analytical definition, have been performed in [24–26].

From [27], the system's natural frequency's for closed-loop electrodes is equal to the location of the zeros in the open-loop system. This means that Equation 3.1 can also be defined as:

$$K_i{}^2 \approx \frac{p_i{}^2 - z_i{}^2}{z_i{}^2} \tag{3.2}$$

with p_i the location of the pole, and z_i the location of the corresponding transmission zero.

This means that the efficiency of the conversion between the electrical energy and the mechanical energy, which also defines the efficiency of the controller, depends on the distance between the relevant pole and transmission zero. How we can optimise the location of the piezoelectric patches according to the pole-zero distance is explained in the following section.

3.2. Pole-zero distance and near-collocation

The transmission zeros of piezoelectric smart structures are important to consider in active damping. These are defined by the SA placement. Unlike the system's poles, as these are an inherent property of the structure and stay unchanged when SA placement changes. In a collocated structure, poles and transmission zeros interlace. This guarantees that the phase stays between $0°$ and $-180°$. This makes it possible to find a fixed-gain controller that guarantees stability for a changing mass and stiffness system, as explained by Preumont[8]. The transmission zero is also relevant for reaching a maximum damping. As controller gains increase, the closed-loop pole moves towards the transmission zero. This extends with the theorem that the maximum reachable damping is dependent on the distance between the pole and the transmission zero. In fact, Preumont[7] defines the maximum damping of the ith mode ξ_i^{max} as:

$$\xi_i^{max} \approx \frac{z_i - \omega_i}{\omega_i} \tag{3.3}$$

This equation applies for lead control where $z_i < 3\omega_i$. The general theorem is easily shown using a root-locus plot of closed-loop systems with increasing pole-zero distance, shown in Figure 3.1.

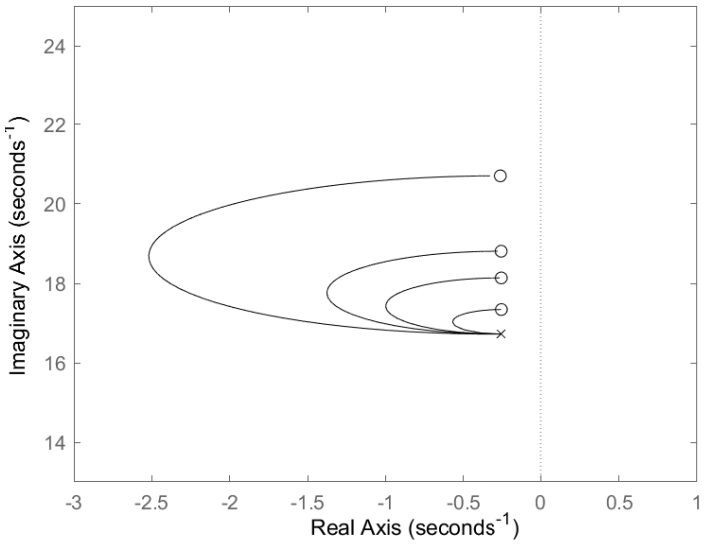

Figure 3.1: Root locus of a DVF compensator with varying transmission zero locations. Notice a larger possible $\xi_i^{max} = -cos(\psi)$ for a larger distance between the pole and transmission zero

Building on this idea, the pole-zero distance can be used as a criterion to optimise SA placement. Such an optimisation was performed for a displacement-force SA pair by [28].

As this paper does not use piezoelectric elements, there is a gap for exploring the possibility of mechanically increasing the pole-zero distance for piezoelectric SA pairs. A hint is given by Preumont [7], where in Chapter 4.8.7 it is shown that near-collocation of piezoelectric elements increases the pole-zero distance.

Using the problem definition defined in 2, it can be shown that near-collocation of piezoelectric SA pairs can increase pole-zero distance. By shifting the location of the sensor relative to the actuator, the SA pair is no longer fully collocated. The system is shown in Figure 3.2. x_1 and x_2 denote the start and end of the piezoelectric actuator, and x denotes the position of the piezoelectric sensor. Both the sensor and the actuator have an equal length L_{pzt}. The length of the cantilever is L. In Table 3.1, the values of these parameters are defined.

Figure 3.2: System definition of the nearly-collocated SA pair simulation. Values in Table 3.1

Table 3.1: Values for the near-collocation simulation defined in Figure 3.2

Variable	Value
L	0.5
L_{pzt}	0.075
x_1	0.05
x_2	0.125

The result of this simulation is shown in Figure 3.3. As can be seen in the (2,2) plot, which is the V_{out}/V_{in} FRF, the transmission zero moves further away from the pole for a larger x. Notice that because the non-collocated FRF at (1,1) (z_{displ}/z_{inp}) has no zeros, no effect is seen in this plot, except for stiffening of some poles, since the piezoelectric patches are stiffening the beam.

As the SA pair becomes less and less collocated, the higher frequency modes become non-collocated, and the phase drops below $-180°$. This is an important observation, as this could cause instability for some controllers, and careful consideration of the controller design is required to guarantee stability for systems with changing masses or stiffness.

Small position differences can have a large effect on the pole-zero distance. In [7], the difference of using Euler-Bernoulli beam theory or a more extensive finite element plate theory is investigated, and it is shown that small positional changes can affect the pole-zero distance by a quite large amount. Because of this, to accurately simulate the effect on near-collocation for large and/or complicated systems, extensive finite element plate model simulation must be performed. For this reason, near-collocation might require relatively much design effort. In Section 4.4, a different method to vary pole-zero distance is discussed, which might offer an more design effort-efficient alternative for complicated systems.

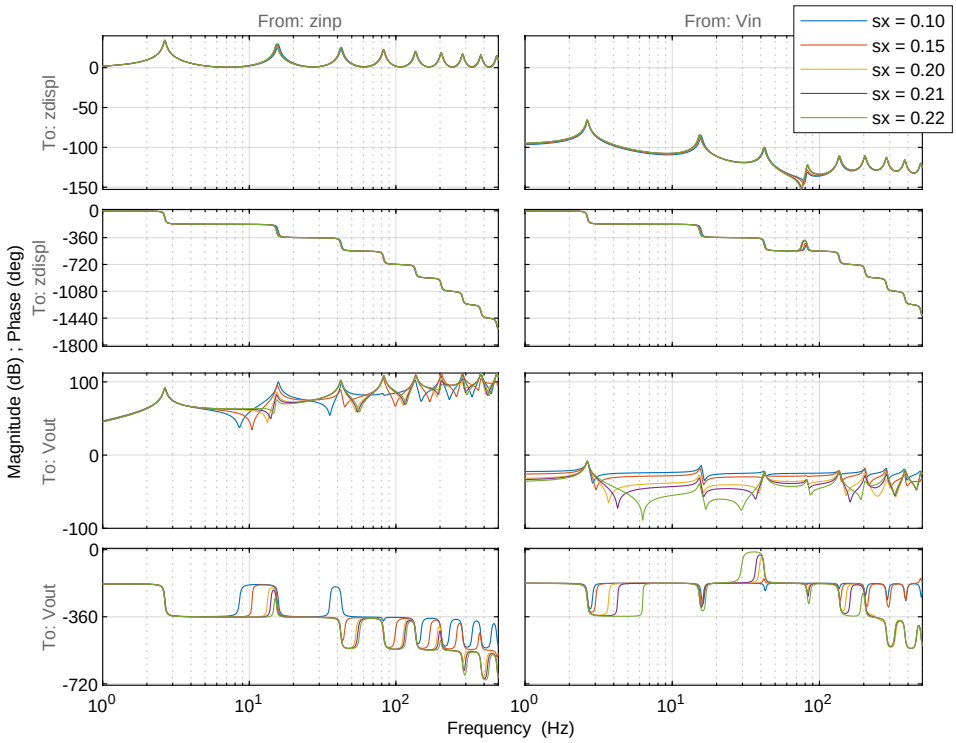

Figure 3.3: MIMO bode plot of a nearly-collocated piezoeletric SA pair with varying actuator placement

4

Controller Design

To control the vibrations of disturbances in the system defined in Chapter 2, a control law is formed such as in Figure 4.1. Negative feedback is assumed. The goal of this control system is to decrease the magnitude of the peaks corresponding to the poles of the plant G. For simple dynamic systems, usually only the first few modes are relevant for most of the disturbance amplifications. Because of this, vibration control in this study is focused only on damping only a certain number of modes.

Preferably, the control system will not change the dynamics of the system beyond these peaks, as this can amplify electronic noise. For this reason, resonant control is a popular option. This type of controller usually consists of a first- or second-order dynamic system (compensator). As this requires relatively low control effort, it is called *Low Authority Control (LAC)*. This is in contrast with controllers that fully change the system dynamics, such as relocating the closed-loop poles (natural frequency and damping). This type of control is called *High Authority Control (HAC)*[7]. *HAC* will be disregarded in this study.

In this chapter, popular effective *LAC* compensators for use in active damping are discussed. Also, IRC and feed-through control is discussed, which is used to increase pole-zero distance and improves active damping performance.

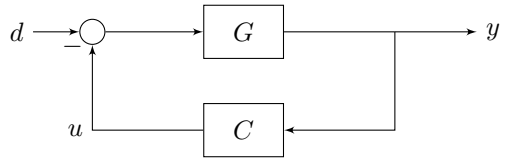

Figure 4.1: The basic control scheme of an Active Vibration Controlled system as described in Chapter 2

4.1. Direct Velocity Feedback

Direct Velocity Feedback [29] (DVF) is a basic form of active vibration control that, as its name suggests, provides direct feedback for a system with velocity output and force input. This provides a 90° phase offset which dampens the modes. The DVF compensator is then defined as

$$H(s) = g_{dvf}s \tag{4.1}$$

where s is the Laplace operator. The differentiating action of the Laplace operator is used as the system in 4.1 uses position sensing instead of velocity sensing. DVF can also be compared to D-control, or as a skyhook damper. Theoretically, it is not affected by the dynamics of the plant structure. In practise, high-frequency spillover can cause spillover problems because DVF has no high-frequency roll-off.

DVF applied to the cantilever problem in Chapter 2 is shown in Figure 4.2. DVF can not be tuned to specific modes, so in its basic form will add an equal amount of damping to each mode. In practise, as can be seen in Figure 4.2b, modes that have lower observability and controllability due to the location of the piezoelectric patches will have a lower reduction in vibration. Also, since the maximum damping

value AVC can reach according to Equation 3.3, the reachable damping will decrease as $\omega \to \infty$. Furthermore, DVF has a great effect on the dynamics of the closed-loop system, mostly on the higher frequencies, since the DVF compensator, as defined in Equation 4.1 increases with frequency. This can be clearly observed in Figure 4.2a.

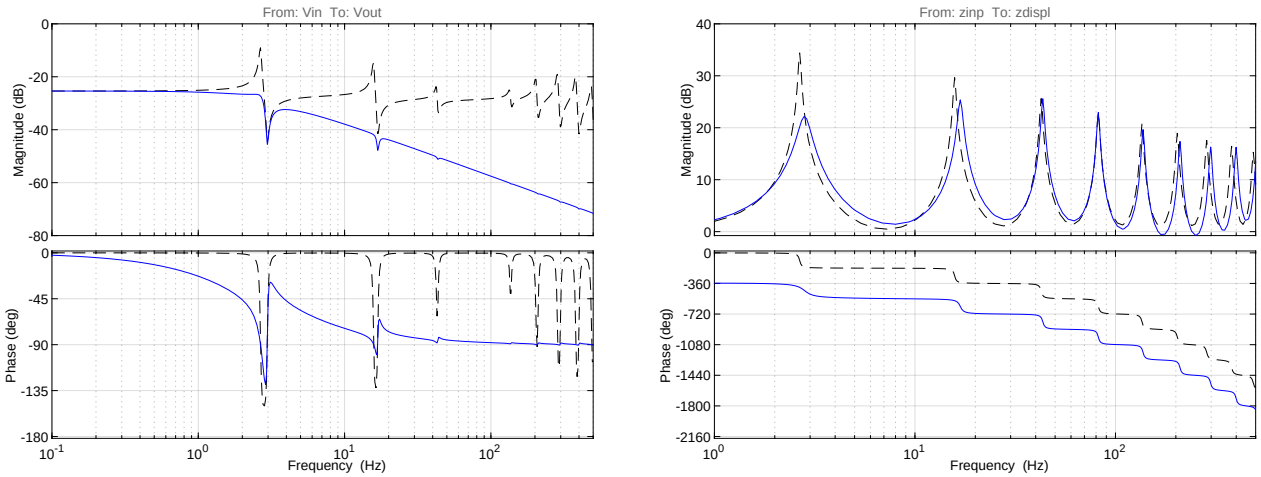

(a) Collocated piezoelectric FRF

(b) Non-collocated objective FRF

Figure 4.2: DVF applied to the simple cantilever system. Dotted: no control. Solid blue: with control

The optimal gain value of the DVF compensator can be investigated in the system's root-locus plot. The root-locus plot of the cantilever example is shown in Figure 4.3. For each pole, the damping ratio is defined as $\xi = -cos(\psi)$ with ψ is the phase of the pole, the highest damping is achieved for the greatest phase. The optimal gain value is read from this plot.

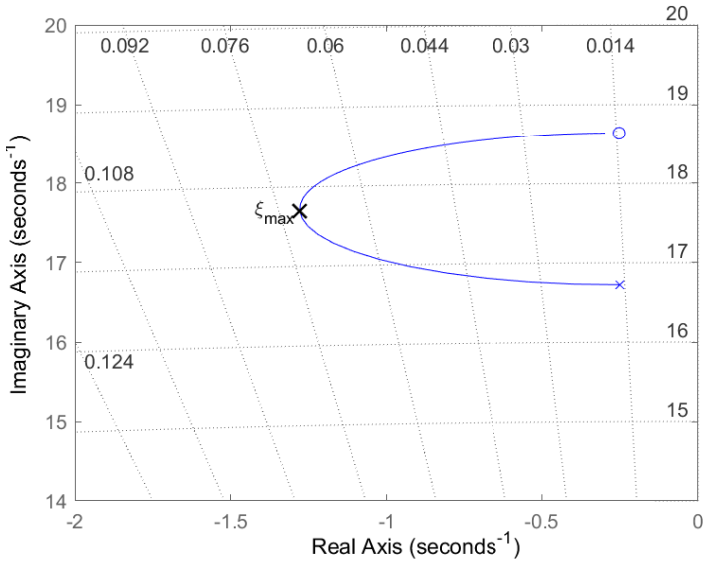

Figure 4.3: Root-locus plot of system with DVF compensator

4.2. Positive Position Feedback

As cantilever systems have unlimited DoF, the modelled system will have unlimited poles. Since this is impossible to model, a maximum number of modes will be modelled. Unmodeled high-frequency modes can cause spillover problems [30] to compensators without high-frequency roll-off. For this reason, Positive Position Feedback was introduced [31]. As PPF is basically a 2nd order low-pass filter, it introduces high-frequency roll-off and thus guarantees stability. The cutoff frequency can be tuned, which makes it a popular option to damp a specific mode. In PPF, the compensator is defined as:

$$H(s) = -\frac{g_c}{\omega_c^2 + 2\zeta_c\omega_c s + s^2}$$

Here, ω_c is the cutoff frequency and the targeted mode. ζ_c is generally between 0.1 and 0.5, but can be optimised for different systems. For equal gain values, a decrease in ζ_c will increase the efficiency of the compensator, since a lower compensator gain g_c is required for the same damping. But for lower values of ζ_c, a small move in system natural frequency will greatly decrease compensator performance. Thus, a higher ζ_c value will increase robustness.

Since PPF has zero slope for $\omega < \omega_c$, the compensator adds steady-state gain to the system. This low-frequency magnitude increase can be clearly seen in Figure 4.5a. To achieve stability according to the Nyquist criteria, the open-loop transfer function must satisfy $L(j\omega) < 1$ at the $\psi(j\omega) = 180°$ crossover point. Since the open-loop FRF will always start at $180°$, the stability condition of a PPF compensator becomes

$$g_c G(j0) \leq 1 \tag{4.2}$$

For a given compensator damping, the gain value can once again be optimised using the root-locus plot of the system, as seen in Figure 4.4. In this Figure the effect of different damping values can also be observed. As can be seen in Figure 4.4, increasing ζ_c will increase the maximum closed-loop damping value ξ_{max}, but as mentioned above, it will require more compensator gain to reach this maximum. As PPF is limited by the stability condition defined by Equation 4.2, there is an optimum between ζ_c and g_c which will reach the maximum reachable ξ_{max}.

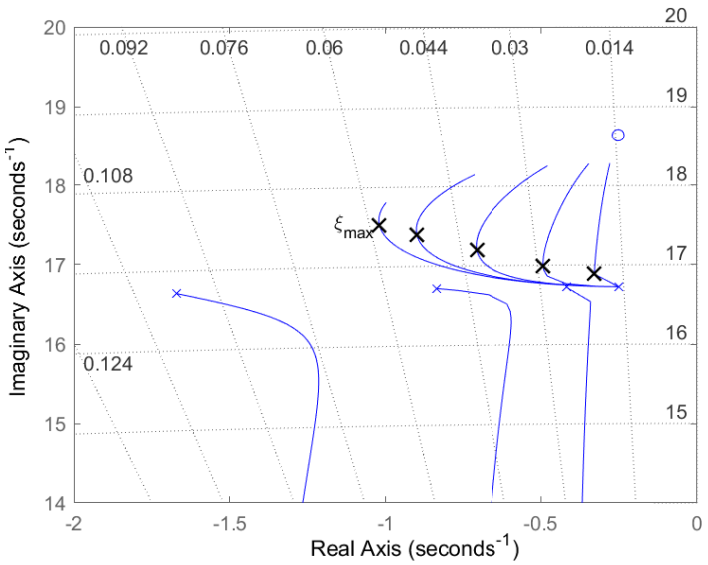

Figure 4.4: Root loci for $\zeta_c = 0.025 \rightarrow 0.4$. For a larger ζ_c, there will be a greater ξ_{max}. The root-locus line stops when the closed-loop system becomes unstable due to high gains.

Targeting multiple eigenmodes is possible with parallel PPF compensators [32]. This introduces tuning issues, as higher-frequency-targeted PPF compensators influence the lower frequency PPF compensators. The effect of a single PPF applied to the problem in Chapter 2, tuned to the first mode, is shown in Figure 4.5. The effect on the steady-state gain ($\omega < \omega_c$) can be observed in Figure 4.5a.

This effect softens the system and decreases gain margin (Equation 4.2). Due to the high-frequency roll-off of PPF, the closed loop dynamics for $\omega > \omega_c$ are unaffected.

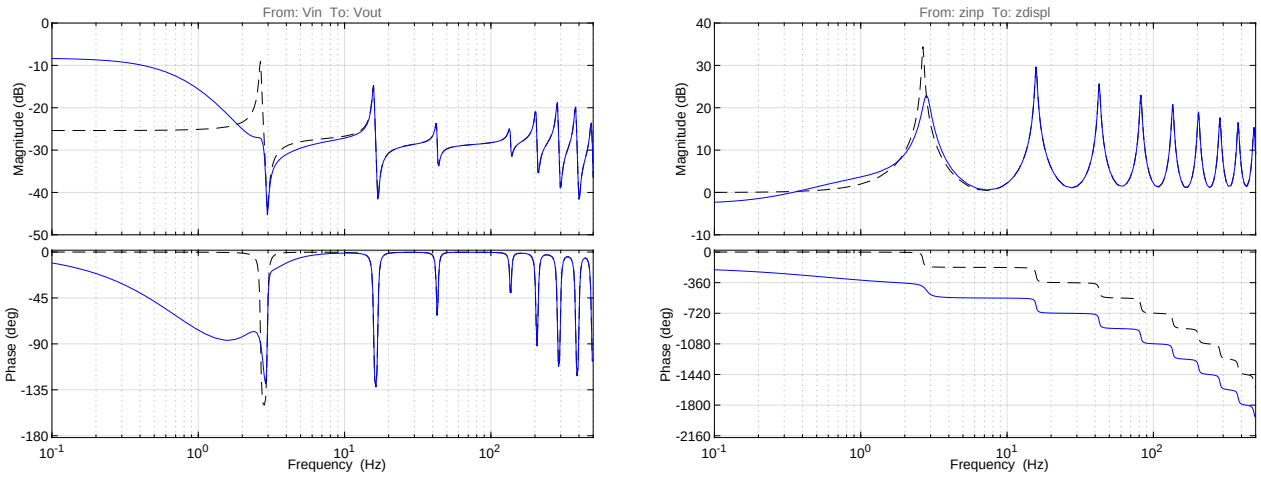

(a) Collocated piezoelectric FRF

(b) Non-collocated objective FRF

Figure 4.5: PPF control with $\zeta = 0.4$ and $g_c = 9.5$ applied to the simple cantilever system. Dotted: no control, solid blue: control

4.3. Negative Position Feedback

Solving spillover issues for DVF, PPF is a popular and robust option for vibration control. But since PPF has no slope for $\omega < \omega_c$, the compensator amplifies low-frequency disturbances. For this reason, it can be unsuitable for targeting higher-frequency nodes. Also, the stability condition limits the performance of the system for higher compensator damping values.

To overcome these problems, [33] introduced Negative Derivative Feedback. The NDF compensator is defined as

$$H_{ndf}(s) = \frac{g_c s}{\omega_c^2 + 2\zeta_c \omega_c s + s^2} \tag{4.3}$$

This compensator is designed for a plant with velocity output. Since piezoelectric elements provide a position output, this cannot be directly copied, as the phase would be exactly 90 degrees offset. By adding a differentiating term, NDF is converted to Negative Position Feedback (NPF), defined by:

$$H_{npf}(s) = \frac{g_c s^2}{\omega_c^2 + 2\zeta_c \omega_c s + s^2} \tag{4.4}$$

[34] compared NPF and PPF on a flexible arm with a piezoelectric actuator, and showed a better performance for NPF. NPF has a better stability margin as it does not increase steady-state gain, so it can theoretically reach better performances than PPF without becoming unstable. As with PPF, the controller damping ζ_c determines the robustness of the controller. Smaller values of ζ_c are more efficient in damping single modes, but a slight shift in the natural frequency of this mode will decrease the performance significantly.

Recently, [35] presented a method of calculating the NDF compensator variables to optimise damping for piezoelectric structures. This method can be defined with control optimisation methods H_2 or H_∞ and can be used to fully optimise NDF compensators for either objectives.

A simple NPF was applied to the example cantilever problem from Chapter 2, with $\zeta_c = 0.8$. The result is shown in Figure 4.6. Observe that NPF affects the closed loop system dynamics for $\omega > \omega_c$, but has no effect on the steady-state value. As with PPF, it is possible to use parallel NPF controllers to target multiple modes.

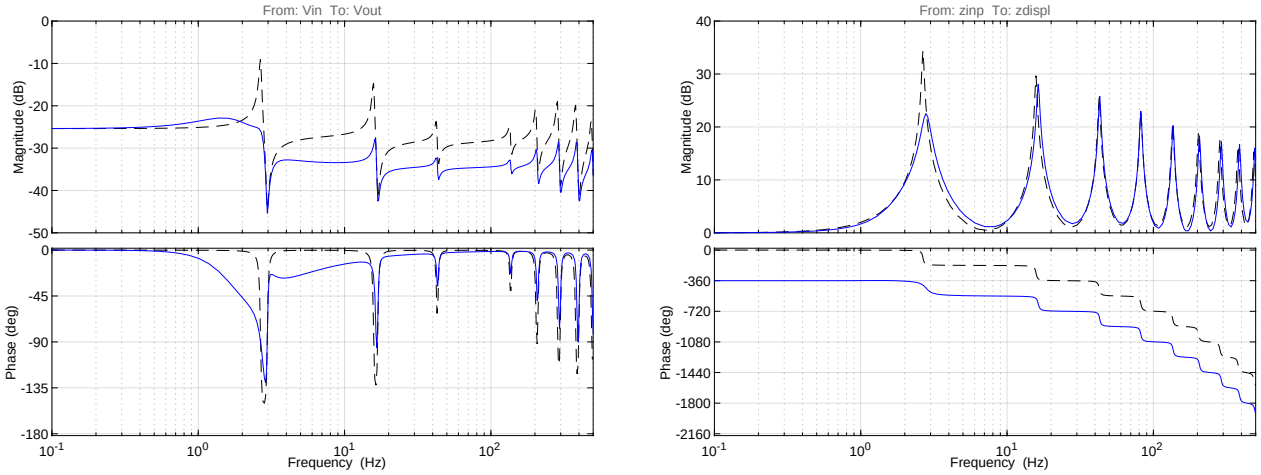

(a) Collocated piezoelectric FRF

(b) Non-collocated objective FRF

Figure 4.6: NPF control targeted at the first mode with $\zeta = 0.8$ and $g_c = 12.6$ applied to the simple cantilever system. Dotted: no control, solid blue: control

4.4. Integral Resonant Control and feed-through control

As explained in Section 3.2, increasing the pole-zero distance of a collocated transfer function can increase the performance of compensators, as they can increase damping values even more. In [36], a method is introduced to increase this distance using control. A constant feed-through term Ft is added parallel to the plant, which feeds a portion of the actuator signal through to the sensor signal, as shown in Figure 4.7. This technique results in the placement of resonant zeros at an arbitrary location in the plant's response function. By placing this zero before the pole, a zero-before-pole collocated transfer function is created, with a phase between $0°$ and $-180°$. Using integral feedback, the poles of this system can consequently be damped. The resulting system has a phase between $-90°$ and $90°$ with infinite gain margin and a $90°$ phase margin.

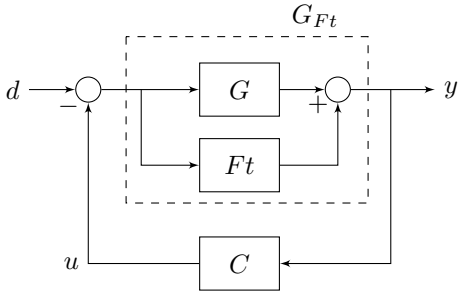

Figure 4.7: Feed through control law

In Integral Resonant Control (IRC), the system with feed-through G_{Ft} is controlled with an integral compensator. In [36], this is done with a zeroth-order, first-order, or second-order integral compensator. The zeroth and first order compensators have very high sensitivity at low frequencies, which can cause actuator saturation for low frequency control action. The second order integral compensator has low-frequency roll-off and greater gain attenuation, but yields phase margin for the closed-loop system.

The second-order compensator is defined as:

$$H_{irc}(s) = \frac{g_c s}{(s+\omega_c)(s+\omega_c)} \tag{4.5}$$

where ω_c falls about a decade below the target mode, to make sure that the open-loop phase at the target mode is $-180°$. Using the root-locus plot, the optimal gain value can be determined.

Since the pole-zero distance can be varied using the feed-through term, IRC is by far the most effective method for damping the first mode. But since the compensator defined in Equation 4.5 falls far below the target mode, it requires very high gain values to fully dampen the target mode. To fix this, it's possible to use other compensators, like DVF, PPF or NPF, on the fed through plant. All combinations are possible, and with every combination, the fed-through plant and compensator combination provides more maximum damping than the normal plant with the same compensator. In Figure 4.8, this difference is clearly observed for DVF.

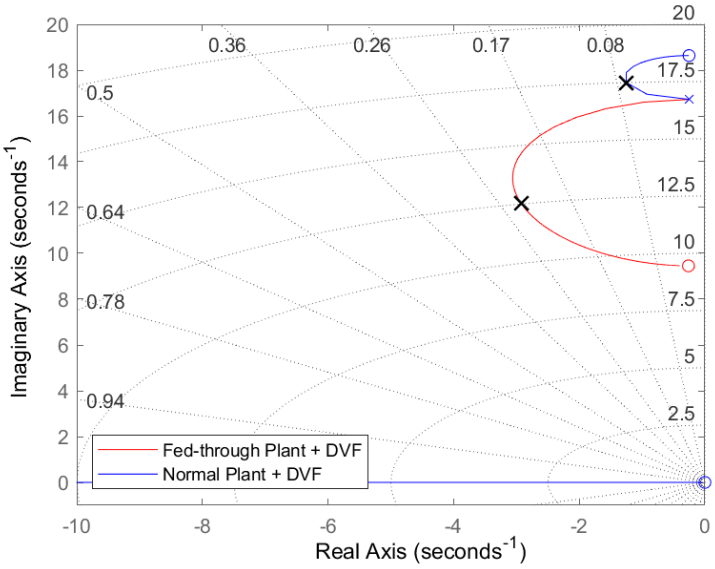

Figure 4.8: Root-locus of fed-through plant with DVF control

5

Performance Metrics and Optimising Design

The performance of an AVC system can be defined in multiple ways and will depend on the constraints and requirements set. Optimising an AVC system starts with knowing how the performance should be defined. The performance metrics and constraints defined in this chapter should help an engineer to design a practically effective AVC system. Also, a practical performance metric is introduced which accounts for electronic noise, which might be amplified by the control loop acting on the system.

5.1. Modal Damping

Reducing vibrations of modes is generally the main focus of AVC. This often means reducing settling time of a system, or damping specific target modes. Since the settling time t_s of a second order system is related to the system's modal damping $2\zeta\omega$, the modal damping of specific modes $2\zeta_i\omega_i$ can be used as system-wide performance metric. To effectively decrease settling time, one might figure out which modes have the greatest influence on the amplifications of the disturbance signal. This can be estimated by looking at the frequency spectrum of the disturbances. In [23], a Specific Damping Index is used where multiple modal damping values are weighed accordingly and summed. This is consequently used as performance index for optimising the system. In most papers about AVC techniques, a modal damping approach to performance is used [34, 36, 37].

For an experimental setup, the plant can be fitted to generate the transfer function of the relevant modes. Using the fitted model, the closed-loop system can be simulated and the damping values can be calculated from this transfer function. This will give a closed-loop performance metric which can be used to optimise the system's mechanics and control. If fitting is not possible or infeasible, numeric models with discrete controllers can also be used to generate a closed-loop FRF. In this case, the quality factor and damping value can be read off the numeric bode plot.

5.2. Dynamic Error Budgeting

Rating performance solely as modal damping can present problems in practise, where electronic noise can deliver an extra error to the system. Controllers may be designed to dampen the system, but can simultaneously amplify electronic noise. Since electronic noise is generated from the sensor/actuator and control system, it is acting through the piezoelectric patches. The transfer of the noise to the tip displacement is defined by the cross-talk transfer functions as explained in Chapter 2. Figure 5.1 shows how the contributions of the cross-talk terms define this transfer. It is also extended with a control loop acting on G_{22}. Also, electronic noise is often acting on different frequencies than the disturbance. This means that high controller gains can increase the electronic noise while decreasing the disturbance, effectively increasing the total dynamic error. The design of an AVC system must account for the increase, or at least presence, of electronic noise by the control law.

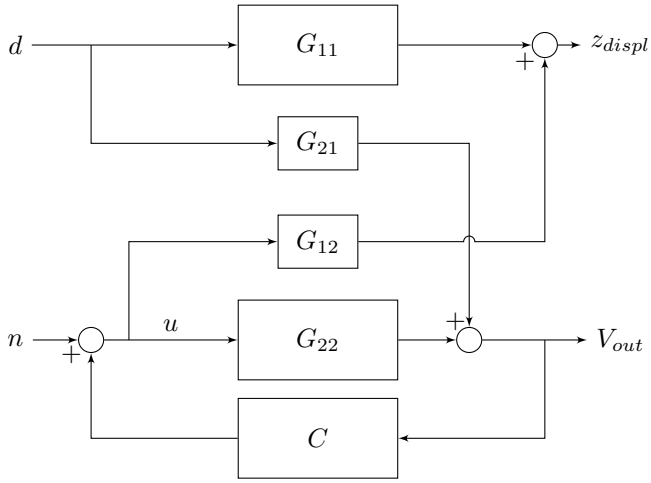

Figure 5.1: Complete decentralised control law including the influences through the cross talk terms

Considering electronic noise, it is possible to use Dynamic Error Budgeting (DEB) to better optimise the total dynamic error [38–40]. As different parts of the system present different amounts of disturbances, DEB can show the contributions of each. To do this, designers require to know the variance and frequency spectrums of the disturbances. For stochastic and normally distributed disturbances, the following functions apply:

$$\text{mean} \qquad \bar{x} = \lim_{T\to\infty} \frac{1}{2T} \int_{-T}^{T} x(t)\mathrm{d}t \tag{5.1}$$

$$\text{power} \qquad \|x\|_{\text{rms}}^2 = \lim_{T\to\infty} \frac{1}{2T} \int_{-T}^{T} x(t)^2\mathrm{d}t \tag{5.2}$$

$$\text{variance} \qquad \sigma_x^2 = \|x-\bar{x}\|_{\text{rms}}^2 = \lim_{T\to\infty} \frac{1}{2T} \int_{-T}^{T} (x(t)-\bar{x})^2\mathrm{d}t \tag{5.3}$$

Which means for zero-mean stochastic disturbances, the power is equal to the variances of the disturbance. The Root Mean Square (RMS) value of the signal is equal to the square root of the variance, or 1σ.

Using Percival Theorem, the time domain power connect to the frequency domain power with the following equation:

$$\|x\|_{\text{rms}}^2 = \lim_{T\to\infty} \frac{1}{2T} \int_{-T}^{T} x(t)^{\mathrm{d}}t = \int_0^{\infty} \mathit{PSD}_x(f)\mathrm{d}f \tag{5.4}$$

Where $\mathit{PSD}_x(f)$ refers to the single-sided power spectral density of $x(t)$ [38]

To find the total influence of a disturbance over the entire frequency spectrum, the PSD is integrated over the frequency to get the Cumulative Power Spectrum Density (CPSD or CPS):

$$\mathit{CPS}(f) = \int_0^f \mathit{PSD}(v)\mathrm{d}v \tag{5.5}$$

Where $\mathit{CPS}(f\to\infty) = \sigma_x^2$.

As defined in Chapter 2, the problem considered in this study is a MIMO system with decentralised SISO control. As DEB has exclusively been used in SISO cases, the principle needs to be extended to apply for the decentralised control problem. As the noise n acts on the control loop and the position disturbance d acts on the cantilever, they each apply differently on the system. In Figure 5.1, the effect of the disturbance and noise on the tip displacement z_{displ} and the sensor voltage V_{out} is shown.

Using Figure 5.1,

$$\frac{z_{displ}}{n} = G_{12}\frac{1}{1+G_{22}} \tag{5.6}$$

$$\frac{z_{displ}}{d} = G_{11} + G_{12}\frac{-C}{1+G_{22}}G_{21} \tag{5.7}$$

These formulas can be used to determine the influence of the disturbance or noise as defined in Figure 5.1. For a measured noise and disturbance, these transfer functions give the error of z_{displ} by n or d. Using DEB, a total error can be calculated. By adding a control loop, the influence of this controller can be determined. An example is shown in Figure 5.2. In this example, DVF is used on the problem defined in Chapter 2. because DVF is not a resonant compensator, it is observed that it greatly amplifies the electronic noise. Even though the disturbance is damped, the total error has still increased because of the increase of electronic noise.

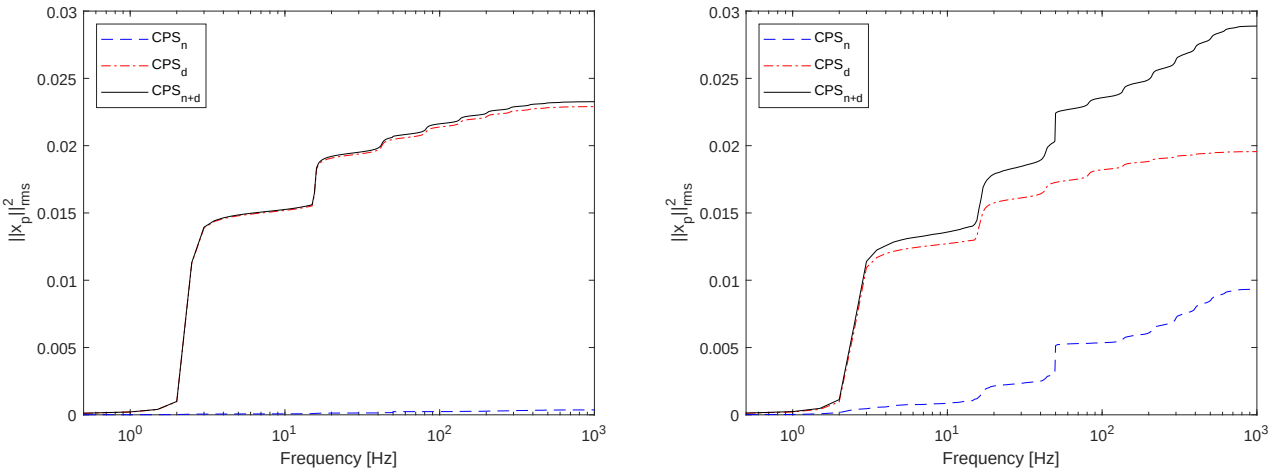

(a) CPSs without control

(b) CPSs with DVF control

Figure 5.2: An example of DEB for the problem given in Chapter 2. The influence of electronic noise amplification by the control loop is clearly shown to increase the total error.

5.3. Constraints

5.3.1. Controller Robustness

Manufacturing tolerances or changes in mass can create a variance in plant dynamics by changing the plant's natural frequencies, damping values, or stiffness lines. These changes can greatly decrease AVC system's effectiveness, as the most effective compensators are often tuned to target modes. Low compensator damping values are highly effective but are easily de-tuned. Control systems with low stability margins also risk destabilisation. To design an effective AVC system, it will have to be designed by taking into account the manufacturing tolerances of the target system. Because manufacturing tolerances are generally normally distributed, the shifting of natural frequencies will also be normally distributed with a mean of μ_ω and standard deviation of σ_ω. To make sure a resonant AVC compensator will satisfy the performance requirements with changing plant dynamics, the engineer must consider the deviation of the target mode's natural frequency, by following the following steps:

1. Tune the resonant compensator (i.e. PPF, NPF, 2nd order IRC, etc) to the target mode's average frequency μ_ω.
2. Determine the resonant compensator's damping ratio, which mostly determines the robustness of the controller, by designing the compensator for a model where the target mode is shifted with a multiple of $\pm\sigma_\omega$. The multiple defines the number of cases where the controller design will satisfy the performance requirement.

If the AVC system has to support a plant with changing mass, for example because the plant is a robot arm which picks up objects, the engineer has to consider the changing plant dynamics to guarantee performance requirement satisfaction. Large changes in plant dynamics might require adaptive control systems [17, 41, 42].

Unmodeled dynamics, such as electronic noise, delay or unknown disturbances, can also destabilise badly designed control systems. Consideration for sufficient gain or phase margins is required to keep the control systems stable and effective. These stability margins can be calculated using the stability conditions for the relevant compensators, defined in Chapter 4.

5.3.2. Actuator saturation

Actuator saturation can limit the performance of any control system and must be considered as a constraint in the optimisation of the AVC system. Looking at Figure 5.1, the control force is defined as u, which is limited by the actuator saturation u_{max}. From [43], u is defined as:

$$u = -d\frac{GC}{1+GC} - n\frac{C}{1+GC} \tag{5.8}$$

As derived from 5.8, it is clear that u depends on the disturbance and noise values d and n. So, for large enough disturbance values, actuator saturation will always occur. To prevent unnecessary actuator saturation, the function $C/(1+GC)$ must be limited at the noise frequency. This can already be achieved by choosing a resonant compensator, which is tuned to the target mode. A designer can also choose the type of controller by looking at the noise frequency. For example, if the target mode has a frequency higher than the frequency made by electronic noise, one can choose NPF instead of PPF, as NPF has a low frequency roll-off. One might also take a look at [44], where an anti-windup compensator is introduced.

6

Conclusion and Research plan

In the following conclusion, research questions from the introduction are answered using the content of this literature study. Finally, a research plan for the thesis is introduced.

1. What are suitable Active Vibration Control (AVC) techniques used for lightly damped structures?

This study includes a review of different techniques that are effective in actively damping lightly damped structures. First, in Chapter 3, the important of the SA placement is explained. Different optimisation criteria are introduced, namely the electromechanical coupling factor and the pole-zero distance of the resulting plant. It is explained how to increase the pole-zero distance of the system with a piezoelectric SA pair. For a more expensive review of SA placement techniques, the reader is referred to [14].

In Chapter 4, the basic control law of AVC is introduced. Then, different compensators are explained. Their effect on the problem in Chapter 2 is investigated and their properties, strengths and weaknesses are explained. In Table 6.1, these compensators are summarised.

All of these techniques, both for SA placement and control, can be suitable for an AVC system for a lightly damped structure. Different combinations of SA placement and compensator might be favourable, explained in Table 6.1. Depending on the system, different combinations will provide varying results. It is important to carefully consider all options and their pros and cons to make an informed decision, preferably backed up with simulations of the complete system.

2. How can the performance of different active vibration control techniques be compared and evaluated for lightly damped structures in terms of metrics such as vibration reduction and robustness?

In Chapter 5, different performance metrics are explained that can be used to compare different AVC techniques. The primary objective of AVC is typically to add damping or decrease settling time. As a result, modal damping is introduced as a performance metric, which is correlated with the settling time of the complete system. Because every mode contributes to a system's settling time, it can be difficult to simulate. In contrast, modal damping of the first few bodes is relatively simple to simulate, which makes it a good performance metric to use for comparing AVC techniques.

In practice, modal damping will not always produce the best performance for AVC systems. This is because electronic noise is usually acting on the system. Because control systems can amplify electronic noise, the total dynamic error of the system can actually increase with poorly designed controllers. In Section 5.2, the effect of the amplification of electronic noise is shown using Dynamic Error Budgeting (DEB). By using Dynamic Error Budgeting, the system can be optimised for minimising the total dynamic error, which includes both process disturbance and electronic noise. This is a realistic method to optimise the actual system performance.

Finally, as a designer might have to account for different design constraints, the effect of common constraints, actuator saturation and robustness/stability, is investigated in Section 5.3. As constraints such as these can often limit system performance, they require accounting for during the design of the AVC system. A specific SA placement or compensator choice might be favoured according to specific constraints.

3. How do the performance of different active vibration control techniques compare for lightly damped structures in terms of metrics such as vibration reduction and robustness?

To achieve maximum damping performance of an AVC system, transmission zeros should certainly be moved further from the system's pole, as discussed in Chapter 3. This can be achieved using near-collocation, which is a possible solution for relatively simple systems without advanced control. As this requires use of a finite element plate model for complicated systems, it might be more useful to achieve the greater pole-zero distance with feed-through control, which is discussed in Section 4.4. In Chapter 4, different compensators are investigated. As resonant compensator offer tuning to a target mode, these are the most efficient to tune specific modes without disturbing system dynamics or amplifying electronic noise. Further, the performance of each technique greatly depends on the type of system and the frequency spectrum of the disturbance and noise sources. Using the performance metrics from Chapter 5, a designer should be able to predict the closed-loop system performance. Table 6.1 gives an overview of each compensator's strengths and weaknesses to make an informed decision for the applied technique.

Table 6.1: Compensators discussed in this study, assuming negative feedback defined in in Figure 4.1

Compensator	Strengths	Weaknesses	Section
Direct Velocity Feedback $H(s) = sg$	• Simple, no tuning required, and damps all mode	• Not a resonant compensator, can not be tuned to a specific mode. • Will damp lower-frequency modes more than higher-frequency modes. • Affects the system dynamics over all frequencies, but mostly at higher frequencies.	4.1
Positive Positional Feedback $H(s) = -\frac{g}{{\omega_c}^2+2\zeta_c\omega_c s+s^2}$	• Does not affect system dynamics at higher frequencies. • Good combination with near-collocation SA placement due to the -2 HF slope roll-off.	• No low-frequency roll-off, hence will soften system and increase steady-state gain • Due to steady-state gain, closed-loop system will become unstable for large gains	4.2
Negative Positional Feedback $H(s) = \frac{gs^2}{{\omega_c}^2+2\zeta_c\omega_c s+s^2}$	• Low-frequency roll-off, does not affect system at lower frequencies. • Can reach higher gains without closed-loop instability unlike PPF	• Affects system dynamics at higher frequencies. • As NPF has no HF roll-off, the combination with near-collocation SA placement risks closed-loop instability.	4.3
Integral Resonant Control 0th Order $H(s) = \frac{g}{s}$	• Works for Zero-pole collocated systems	• As it has no LF roll-off, this compensator risks actuator saturation for low frequency control forces	4.4
Integral Resonant Control 1st Order $H(s) = \frac{g}{s+\omega_c}$	• Has a steady-state value like PPF, which helps prevent actuator saturation.	• Cannot be tuned exactly to a specific mode. As the phase of this compensator goes from $+90°$ to $-90°$, it must be tuned to a frequency around a decade below the first mode. Can't effectively be tuned to a different mode, as it severely changes system dynamics • Requires very high gains for effective damping	4.4
Integral Resonant Control 2nd Order $H(s) = \frac{gs}{(\omega_c+s)(\omega_c+s)}$	• Low-frequency roll-off reduces the chance for actuator saturation	• Requires more gain than it's 1st and 0th order variants • Like it's 1st order variant, cannot be tuned to a specific mode. • Requires very high gains for effective damping	4.4

6.1. Research Plan

The goal of the thesis is to figure out which of the selected active vibration control techniques is most suitable for the VDL ETG wafer handler case study as explained in Section 1.1. The AVC techniques presented in this literature study will be applied to the case study in the remainder of the thesis. An informed choice for the applied damping technique will be made using system simulations. An hypothesis will be formed about the performance and the system will be validated using an experimental setup. For experimental validation, the following experiments will be performed:

1. Noise and disturbance measurements will be performed to provide a basis for Dynamic Error Budgeting to compare the total system performance as explained in Section 5.2.
2. An extensive system identification will be performed to provide a basis for simulating the effect of different compensators and techniques.
3. Closed-loop experiments with different compensators will be performed to validate the hypotheses for the performance of these corresponding techniques explained in Chapter 4. The effect of feed-through control on the performance will be tested.
4. Different sensor locations will be tested to test the effect of near-collocation on the plant's pole-zero distance as explained in Section 3.2.

References

[1] Christian Ucke and H. Joachim Schlichting. “Oscillating Dolls and Skyscrapers”. In: *Phisik in unserer Zeit* 39.1 (2008), pp. 139–141. URL: http://www.ucke.de/christian/physik/ftp/lectures/TMD_English.pdf.

[2] Sang Myeong Kim, Semyung Wang, and Michael J. Brennan. “Dynamic analysis and optimal design of a passive and an active piezo-electrical dynamic vibration absorber”. In: *Journal of Sound and Vibration* 330.4 (Feb. 2011), pp. 603–614. ISSN: 0022460X. DOI: 10.1016/j.jsv.2010.09.004.

[3] T T Soong and Michael C Constantinou. *Passive and Active Structural Vibration Control in Civil Engineering*. Ed. by T. T. Soong and M. C. Costantinou. Vol. 345. Vienna: Springer Vienna, 1994. ISBN: 978-3-211-82615-7. DOI: 10.1007/978-3-7091-3012-4.

[4] S. Nima Mahmoodi, Mohammad Rastgaar Aagaah, and Mehdi Ahmadian. “Active vibration control of aerospace structures using a modified Positive Position Feedback method”. In: *2009 American Control Conference*. IEEE, 2009, pp. 4115–4120. ISBN: 978-1-4244-4523-3. DOI: 10.1109/ACC.2009.5159955.

[5] M. Benosman and G. Le Vey. “Control of flexible manipulators: A survey”. In: *Robotica* 22.5 (Sept. 2004), pp. 533–545. ISSN: 0263-5747. DOI: 10.1017/S0263574703005642.

[6] Weichao Sun, Huijun Gao, and Peng Shi. *Advanced Control for Vehicle Active Suspension Systems*. Vol. 1. 2020. ISBN: 978-3-030-15785-2.

[7] André Preumont. *Vibration control of active structures*. Vol. 4th. 2018.

[8] A Preumont. *Mechatronics Dynamics of Electromechanical and Piezoelectric Systems*. Vol. 136. 2006. ISBN: 1-4020-4695-2.

[9] Wei He and Jinkun Liu. *Active Vibration Control and Stability Analysis of Flexible Beam Systems*. 2019. ISBN: 978-981-10-7538-4.

[10] Moon Kyu Kwak. *Dynamic Modeling and Active Vibration Control of Structures*. Springer Netherlands, 2022. DOI: 10.1007/978-94-024-2120-0.

[11] Nader Jalili. *Piezoelectric-based vibration control: From macro to micro/nano scale systems*. Springer US, 2010, pp. 1–517. ISBN: 9781441900692. DOI: 10.1007/978-1-4419-0070-8.

[12] Wodek K. Gawronski. *Mechanical Engineering Series*. 2004. ISBN: 0-387-40649-2.

[13] Manal El Ajjaj. *Vibration suppression of a state-of-the-art wafer gripper*. 2022. URL: https://repository.tudelft.nl/islandora/object/uuid%3A671bba53-1a84-4c64-9d3b-ef4319f0e1c1.

[14] Vivek Gupta, Manu Sharma, and Nagesh Thakur. *Optimization criteria for optimal placement of piezoelectric sensors and actuators on a smart structure: A technical review*. Aug. 2010. DOI: 10.1177/1045389X10381659.

[15] A. Hać and L. Liu. “Sensor And Actuator Location In Motion Control Of Flexible Structures”. In: *Journal of Sound and Vibration* 167.2 (Oct. 1993), pp. 239–261. ISSN: 0022460X. DOI: 10.1006/jsvi.1993.1333.

[16] K. B. Lim. “Method for optimal actuator and sensor placement for large flexible structures”. In: *Journal of Guidance, Control, and Dynamics* 15.1 (Jan. 1992), pp. 49–57. ISSN: 0731-5090. DOI: 10.2514/3.20800.

[17] Fujun Peng, Alfred Ng, and Yan-Ru Hu. “Actuator Placement Optimization and Adaptive Vibration Control of Plate Smart Structures”. In: *Journal of Intelligent Material Systems and Structures* 16.3 (Mar. 2005), pp. 263–271. ISSN: 1045-389X. DOI: 10.1177/1045389X05050105.

[18] A M Sadri, J R Wright, and R J Wynne. “Modelling and optimal placement of piezoelectric actuators in isotropic plates using genetic algorithms”. In: *Smart Materials and Structures* 8.4 (Aug. 1999), pp. 490–498. ISSN: 0964-1726. DOI: 10.1088/0964-1726/8/4/306.

[19] I. Bruant and L. Proslier. “Optimal location of actuators and sensors in active vibration control”. In: *Journal of Intelligent Material Systems and Structures* 16.3 (Mar. 2005), pp. 197–206. ISSN: 1045389X. DOI: 10.1177/1045389X05047989.

[20] S.O.R. Moheimani and T. Ryall. “Considerations on placement of piezoceramic actuators that are used in structural vibration control”. In: *Proceedings of the 38th IEEE Conference on Decision and Control (Cat. No.99CH36304)*. IEEE, pp. 1118–1123. ISBN: 0-7803-5250-5. DOI: 10.1109/CDC.1999.830077.

[21] Isabelle Bruant, Laurent Gallimard, and Shahram Nikoukar. “Optimal piezoelectric actuator and sensor location for active vibration control, using genetic algorithm”. In: *Journal of Sound and Vibration* 329.10 (2010), pp. 1615–1635. ISSN: 10958568. DOI: 10.1016/j.jsv.2009.12.001.

[22] Santosh Devasia et al. “Piezoelectric actuator design for vibration suppression - Placement and sizing”. In: *Journal of Guidance, Control, and Dynamics* 16.5 (Sept. 1993), pp. 859–864. ISSN: 0731-5090. DOI: 10.2514/3.21093.

[23] Young Kyu Kang et al. “Optimum Placement of Piezoelectric SensorActuator for Vibration Control of Laminated Beams”. In: *AIAA JOURNAL* 34.9 (1996). DOI: 10.2514/3.13326. URL: http://arc.aiaa.org.

[24] S M Yang et al. “Optimization of noncollocated sensor/actuator location and feedback gain in control systems”. In: *Smart Mater. Struct* 2 (1993), p. 96. DOI: 10.1088/0964-1726/2/2/005.

[25] Yaowen Yang Ã, Zhanli Jin, and Chee Kiong Soh. “Integrated optimal design of vibration control system for smart beams using genetic algorithms”. In: *JOURNAL OF SOUND AND VIBRATION* 282 (2005), pp. 1293–1307. DOI: 10.1016/j.jsv.2004.03.048. URL: www.elsevier.com/locate/jsvi.

[26] Guoliang Xia et al. “Vibration suppression with optimal sensor/actuator location and feedback gain”. In: *Smart Mater. Struct* 2 (1993), pp. 232–239. DOI: 10.1088/0964-1726/2/4/004.

[27] Shashank Pathak et al. “On transmission Zeros of piezoelectric structures”. In: *Journal of Intelligent Material Systems and Structures* 33.12 (July 2022), pp. 1538–1561. ISSN: 15308138. DOI: 10.1177/1045389X211057209.

[28] Dimitri Piron et al. “A pole-zero based criterion for optimal placement of collocated sensor-actuator pair”. In: *Mechanical Systems and Signal Processing* 155 (June 2021). ISSN: 10961216. DOI: 10.1016/j.ymssp.2020.107533.

[29] Mark J. Balas. “Direct Velocity Feedback Control of Large Space Structures”. In: *Journal of Guidance and Control* 2.3 (May 1979), pp. 252–253. ISSN: 0162-3192. DOI: 10.2514/3.55869.

[30] M. J. Balas. “Active control of flexible systems”. In: *Journal of Optimization Theory and Applications* 25.3 (July 1978), pp. 415–436. ISSN: 0022-3239. DOI: 10.1007/BF00932903.

[31] C. J. Goh and T. K. Caughey. “On the stability problem caused by finite actuator dynamics in the collocated control of large space structures”. In: *International Journal of Control* 41.3 (Mar. 1985), pp. 787–802. ISSN: 0020-7179. DOI: 10.1080/0020718508961163.

[32] Madhan Gopal and Muruganandam Mallur. *A comparative study on distributed active damping of flexible systems*. 2020. URL: https://repository.tudelft.nl/islandora/object/uuid%3Ad8a3667d-14df-4b79-a5d9-c3f1a23d5b5e.

[33] G. Cazzulani et al. “Negative derivative feedback for vibration control of flexible structures”. In: *Smart Materials and Structures* 21.7 (July 2012). ISSN: 09641726. DOI: 10.1088/0964-1726/21/7/075024.

[34] Hassaan Hussain Syed. “Comparative study between positive position feedback and negative derivative feedback for vibration control of a flexible arm featuring piezoelectric actuator”. In: *International Journal of Advanced Robotic Systems* 14.4 (July 2017), pp. 1–9. ISSN: 17298814. DOI: 10.1177/1729881417718801.

[35] Rasa Jamshidi and Christophe Collette. “Optimal negative derivative feedback controller design for collocated systems based on H2 and H∞ method”. In: *Mechanical Systems and Signal Processing* 181 (Dec. 2022). ISSN: 10961216. DOI: 10.1016/j.ymssp.2022.109497.

[36] Sumeet S. Aphale, Andrew J. Fleming, and S. O. Reza Moheimani. “Integral resonant control of collocated smart structures”. In: *Smart Materials and Structures* 16.2 (Apr. 2007), pp. 439–446. ISSN: 09641726. DOI: 10.1088/0964-1726/16/2/023.

[37] Ladislav Starek and Stefan Fenik. “Optimal PPF Controller for Multimodal Vibration Suppression”. In: *Engineering MECHANICS* 15.3 (2008), pp. 153–173. URL: http://www.engineeringmechanics.cz/pdf/15_3_153.pdf.

[38] Leon Jabben and Jan van Eijk. “Performance analysis and design of mechatronic system”. In: *DEB Mikroniek* 51.2 (2011), pp. 5–12.

[39] Rudolf Saathof et al. “Integrated system and control design of a one DoF nano-metrology platform”. In: *Mechatronics* 47 (Nov. 2017), pp. 88–96. ISSN: 09574158. DOI: 10.1016/j.mechatronics.2017.08.013.

[40] Wouter Monkhorst. *Dynamic Error Budgeting a design approach*. 2004. URL: https://repository.tudelft.nl/islandora/object/uuid%3A073a04ec-6cb6-4e08-854f-8f063a7aaa44.

[41] Hani I M Alhasni. *Adaptive Multimodal Damping of Flexible Structures*. 2021. URL: https://repository.tudelft.nl/islandora/object/uuid%3Abd489d85-8e4b-4176-b2a6-a6a17d3805f1.

[42] M A Hossain and M O Tokhi. “Evolutionary adaptive active vibration control”. In: *Journal of Systems and Control Engineering* 211.3 (1997). DOI: https://doi.org/10.1243/0959651971539722.

[43] Robert Munnig Schmidt et al. *The Design of High Performance Mechatronics*. 3rd ed. 2020. ISBN: 9781614993674.

[44] Sami Tliba and Matthieu Varnier. “Dealing with actuator saturation for active vibration control of a flexible structure piezo-actuated”. In: *2010 IEEE International Conference on Control Applications*. IEEE, Sept. 2010, pp. 1743–1748. ISBN: 978-1-4244-5362-7. DOI: 10.1109/CCA.2010.5611182.